UNIVERSIDADE ESTADUAL DE CAMPINAS
Instituto de Geociências

Jackeline Monteiro Faustinoni

MIGMATITOS DO COMPLEXO XINGU NA PORÇÃO NORDESTE DOMÍNIO CARAJÁS, CRÁTON AMAZÔNICO, BRASIL.

CAMPINAS
2017

JACKELINE MONTEIRO FAUSTINONI

MIGMATITOS DO COMPLEXO XINGU NA PORÇÃO NORDESTE DOMÍNIO CARAJÁS, CRÁTON AMAZÔNICO, BRASIL.

DISSERTAÇÃO APRESENTADA AO INSTITUTO DE GEOCIÊNCIAS DA UNIVERSIDADE ESTADUAL DE CAMPINAS PARA OBTENÇÃO DO TÍTULO DE MESTRA EM GEOCIÊNCIAS, NA AREA DE GEOLOGIA E RECURSOS NATURAIS

ORIENTADORA: PROFA. DRA. CAROLINA PENTEADO NATIVIDADE MORETO
COORIENTADOR: PROF. DR. ROBERTO PEREZ XAVIER

ESTE EXEMPLAR CORRESPONDE À VERSÃO FINAL DA DISSERTAÇÃO/TESE DEFENDIDA PELA ALUNA JACKELINE MONTEIRO FAUSTINONI E ORIENTADA PELA PROFA. DRA. CAROLINA PENTEADO NATIVIDADE MORETO.

CAMPINAS
2017

Agência(s) de fomento e nº(s) de processo(s): CAPES

Ficha catalográfica
Universidade Estadual de Campinas
Biblioteca do Instituto de Geociências
Marta dos Santos - CRB 8/5892

F275m

Faustinoni, Jackeline Monteiro, 1990-
Migmatitos do Complexo Xingu na porção nordeste Domínio Carajás, Cráton Amazônico, Brasil. / Jackeline Monteiro Faustinoni. – Campinas, SP : [s.n.], 2017.

Orientador: Carolina Penteado Natividade Moreto.
Coorientador: Roberto Perez Xavier.
Dissertação (mestrado) – Universidade Estadual de Campinas, Instituto de Geociências.

1. Migmatito. 2. Carajás, Serra dos (PA). 3. Geoquímica. 4. Geocronologia. I. Moreto, Carolina Penteado Natividade,1985-. II. Xavier, Roberto Perez,1958-. III. Universidade Estadual de Campinas. Instituto de Geociências. IV. Título.

Informações para Biblioteca Digital

Título em outro idioma: Migmatites of the Xingu Complex in the northeastern portion Carajás Domain, Amazon Craton, Brazil.
Palavras-chave em inglês:
Migmatite
Carajás, Serra dos (PA)
Geochemistry
Geochronology
Área de concentração: Geologia e Recursos Naturais
Titulação: Mestra em Geociências
Banca examinadora:
Carolina Penteado Natividade Moreto [Orientador]
Vinícius Tieppo Meira
Valdecir de Assis Janasi
Data de defesa: 23-08-2017
Programa de Pós-Graduação: Geociências

UNIVERSIDADE ESTADUAL DE CAMPINAS
INSTITUTO DE GEOCIÊNCIAS

AUTORA: Jackeline Monteiro Faustinoni

Migmatitos do Complexo Xingu na porção nordeste
Domínio Carajás, Cráton Amazônico, Brasil

ORIENTADORA: Profa. Dra. Carolina Penteado Natividade Moreto

Aprovado em: 23 / 08 / 2017

EXAMINADORES:

Profa. Dra. Carolina Penteado Natividade Moreto - Presidente

Prof. Dr. Vinícius Tieppo Meira

Dr. Valdecir de Assis Janasi

A Ata de Defesa assinada pelos membros da Comissão Examinadora, consta no processo de vida acadêmica do aluno.

Campinas, 23 de agosto de 2017.

SÚMULA CURRICULAR

Jackeline Monteiro Faustinoni

É geóloga (2014) pela Universidade Estadual de Campinas. Tem experiência na área de Geociências, com ênfase em mapeamento, petrografia e petrologia de rochas ígneas e metamórficas, geocronologia e evolução crustal. Atuou como auxiliar didático em diversas disciplinas da Graduação em Geologia pela UNICAMP, incluindo Elementos de Geologia, Mineralogia II, Petrologia e Petrografia Ígnea e Petrologia e Petrografia Metamórfica.

Atualmente finaliza o mestrado na área de Geociências pela Universidade Estadual de Campinas com ênfase em estudos petrogenéticos em migmatitos do Complexo Xingu na porção nordeste do Domínio Carajás com base na caracterização petrográfica, geoquímica e geocronológica. Durante o mestrado publicou um artigo em periódico nacional (Qualis B1), dois resumos em congressos nacionais como primeira autora e dois resumos em co-autoria, sendo um deles publicação internacional.

AGRADECIMENTO

Agradeço ao apoio da minha família nessa jornada acadêmica, minha mãe, Mônica, minha vozi, Sueli e meu pai, Sérgio, que juntos me proporcionaram a liberdade de escolher esse caminho, suportaram meus aborrecimentos e minha ausência e sempre ofereceram incentivo nos momentos de desespero.

Aos irmãos, Giovanna e Gabriel, pela parceria eterna e força fraterna e ao irmão, Lorenzo, pela alegria infante.

À companheira Nathalia pelo apoio na conclusão dessa etapa e parceria no incerto porvir.

Aos amigos, que são muitos, e se cansaram de me ouvir falar sobre o mestrado. A presença de cada um me ajudou a continuar e chegar nesse ponto. Obrigada, Juliana, Camila, Gabriela, Mesquita, Daiana, Eduardo, Matheus, Oton, Marcela, Arthur, Isabela. Obrigada a todos os colegas da pós-graduação por compartilharem suas experiências e conhecimento.

Agradecimento imensurável à minha orientadora, Carol, pelo crédito e disponibilidade no início desse projeto e por toda ajuda e suporte nos últimos anos. Aos parceiros de campo e metamorfismo, Lena e Marco, que há tempos me apresentaram as belezas das rochas de alto grau e me ajudaram em todas as etapas desse projeto. Aos professores Lena e Vinícius, pela revisão precisa e sugestões no exame de qualificação. Ao professor Wagner, pela ajuda na petrografia.

À toda equipe do Instituto de Geociências, Valdirene, Gorete, Cristina, Valdir, Margareth, Lúcia, Érica, Dailto e Aparecida pelo suporte administrativo e laboratorial.

Ao prof. Dr. Davis C. de Oliveira (UFPA) pelo apoio logístico na etapa de Campo.

Poderia agradecer a Capes pela bolsa de mestrado, mas considerando essa página como uma oportunidade de expressão livre e o fato de que não vejo grande sentido em ser grata a um órgão de administração pública, sinto-me, então, a vontade para agradecer aqueles que trabalham e defendem a educação pública.

“Downpressor man, where you gonna run to?

You gonna run to the rocks, the rocks will be melting.”

(Peter tosh)

RESUMO

Este estudo examina as relações de campo e a petrografia de ortognaisses e migmatitos atribuídos ao Complexo Xingu na porção nordeste do Domínio do Carajás. Adicionalmente, dados geoquímicos e geocronológicos são apresentados visando uma melhor compreensão da natureza e significado do evento de anatexia durante a evolução mesoarqueana do Domínio Carajás. Dentre os litotipos estudados, o Ortognaisse bandado Xingu corresponde à rocha de mais alto grau metamórfico e com menor conteúdo de leucossoma. A paragênese das bandas anfibolíticas do Ortognaisse Xingu (diopsídio-hornblenda-labradorita) sugere metamorfismo em condições de facies de anfibolito superior. Os migmatitos do Complexo do Xingu estão bem expostos em duas localidades, correspondentes às pedreiras Britalider e Britamil. Esses migmatitos são espacialmente e temporalmente relacionados entre si, embora individualmente formem um amplo espectro entre metatexitos e diatexitos, cujas partes constituintes variam de acordo com a rocha fonte e taxas de fusão. Os tipos de rochas dominantes na pedreira Britalider são anfibolitos e metatonalitos a trondhjemitos estruturados como: i) *patch* metatexito; ii) metatexito estromático; iii) *schollen* diatexito e iv) *schlieren* diatexito. Já na pedreira Britamil, os litotipos predominantes são gnaisses de composição tonalítica, metagranodioritos e anfibolitos estruturados como: i) metatexito estromático e ii) diatexito nebulítico a *schlieren* diatexitos. Em comparação com a pedreira Britalider, o Migmatito Xingu na pedreira Britamil revela taxas de fusão mais baixas, uma vez que o paleossoma anfibolítico não apresenta evidências de fusão e o acúmulo de leucosoma como diatexitos é menos expressivo. Na pedreira Britamil, o Hercynita-Cordierita Gnaisse registra um evento metamórfico de alta temperatura, possivelmente em condições de fácies granulito, em ca 2,88 Ga. A diversidade petrológica encontrada nesses migmatitos exemplifica como a presença de água e taxas de deformação são tão determinantes quanto a composição do protólito e a temperatura durante a fusão das rochas de alto grau. As relações de campo e a petrografia sugerem que o Ortognaisse bandado Xingu provavelmente representa a rocha parental do Migmatito Xingu na pedreira Britalider. O Migmatito Xingu na pedreira de Britamil, preserva o gnaisse tonalítico como mesosoma, sugerindo que seu protolito mais próximo corresponderia a um típico gnaisse cinza arqueano. O Gnaisse tonalítico (mesosoma) da pedreira Britamil apresenta severo empobrecimento de HREE, alta razão La/Yb e baixo Y, afinidade semelhante à série TTG. Ênfase é dada à petrografia de detalhe, que em conjunto com a geoquimica de rocha total e geocronologia U-Pb em zircão fornecem evidências de que as rochas do embasamento mesoarqueano de Carajás sofreram fusão parcial em ca. 2,86 Ga

Palavras-chave: Migmatitos, Mesoarqueano, Domínio Carajás.

ABSTRACT

This work examines field relationship and petrography of migmatites at the northeastern part of the Carajás Domain, Amazon Craton, and presents new geochemical and geochronological data in order to contribute to understanding the nature and significance of anatexis during the mesoarchean evolution of Carajás Domain. Regionally, in the northeastern Carajás area, the Xingu banded Orthogneiss corresponds to the highest metamorphic-grade rock with minimum leucosome content among the studied litotypes. The mafic layers are clinopyroxene-bearing amphibolite with calcium-rich plagioclase in paragenesis, suggesting at least upper amphibolite facies metamorphism. The migmatites of the Xingu Complex are well exposed in two localities, the Britalider and the Britamil quarries. These migmatites are spatial and temporally related though individually form a complex relationship spectrum from metatexites to diatexites, in which the constituent parts varies according to the source-rock and melting rates. The dominant rock types at the Britalider Quarry are amphibolite and metatonalite to trondhjemite structured as i) patch metatexite; ii) stromatic metatexite; iii) schollen diatexite and iv) schlieren diatexite. The predominant rock types at Britamil quarry are a light-gray tonalite gneiss, a metagranodiorite, and an amphibolite, which are structured as i) stromatic metatexite and ii) nebulitic to schlieren diatexite migmatites. In comparison to the Britalider Quarry, the Britamil migmatite reveals lower melting rates, as amphibolite paleosome remained unmelted during anatexis and melt accumulation as diatexites are less expressive. In the Britamil quarry, a high-temperature event at ca 2.88 Ga is registered in zircon grains of a Hercynite-Cordierite–bearing gneiss, which might represent a retrogressed granulite. The petrological diversity produced in these migmatites occurrences provide examples of how the water content and strain rates are as determinant as the protolith composition and temperature in melting of high-grade rocks. Field relationships and detailed petrography strongly suggest that the Xingu banded Orthogneiss most likely represent a parental gneiss of the Xingu migmatites at Britalider Quarry. The comparison of geochemical igneous fingerprints of the mafic layers of the Xingu banded Orthogneiss and the Britalider quarry amphibolite mesosome is not conclusive, though suggests a petrogenetic link between these units. The Xingu migmatites at Britamil quarry preserve the tonalite gneiss mesosome, suggesting that the metatexite closest protolith was a composite gray gneiss. The Tonalite gneiss mesosome presents severe HREE depletion, high La/Yb ratio and low Y, which indicate a TTG series affinity for its igneous protolith. Emphasis was given to detailed petrography and microstructural analysis, which in addition to whole rock geochemistry and U-Pb zircon geochronology data provide evidence that the Carajás mesoarchean basement rocks underwent partial melting at ca 2.86 Ga.

Keywords: Migmatites, Mesoarchean, Carajás Domain.

SUMÁRIO

INTRODUÇÃO

Complexos gnáissicos-migmatíticos são reconhecidos em terrenos arqueanos, como a Província Superior, no Canadá (Sawyer 2008), o Complexo de Itsaq, na Groelândia (Nutman *et al*. 2007) e o Cráton do Kapvaal, no sul da África (Kröner *et al*. 1996). Nessas províncias são encontrados granulitos e granitóides associados a migmatitos, rochas formadas pela fusão parcial da crosta em grandes profundidades e elevadas temperaturas (>650ºC), em condições semelhantes às observadas em orógenos modernos (Sawyer *et al.* 2011). O estudo de rochas de alto grau metamórfico tem especial interesse pois revela processos atuantes na crosta inferior e em sua interface com o manto superior.

O embasamento do Domínio Carajás é composto por ortogranulitos, atribuídos ao complexo Pium; ortognaisses migmatíticos de composição tonalítica a granodiorítica e granitos de afinidade cálcio-alcalina, atribuídos ao complexo Xingu (Silva *et al*. 1974; Hirata *et al*. 1982; Araújo *et al*. 1988; DOCEGEO, 1988; Machado *et al.* 1991). Estudos recentes indentificaram unidades litológicas mesoarqueanas distintas das rochas metamórficas de alto grau (e.g., granitos, rochas metavulcânicas ácidas e metaultramáficas) em áreas antes atribuídas ao Complexo Xingu (e.g., Moreto et al. 2011; 2014, Feio et al 2013), restringindo a ocorrência desse complexo na Província Carajás.

No que diz respeito à evolução do embasamento do Domínio Carajás, Feio *et al*. (2013) sugerem a existência de uma crosta não juvenil (valores εNd negativos) existente ao menos desde o Mesoarqueano (3,2-3,0 Ga). Machado *et al*. (1991) registra a existência de pelo menos dois eventos de migmatização na região de Curionópolis, mas não apresenta a caracterização petrográfica dos migmatitos observados. Segundo Machado *et al.* (1991), o metamorfismo dos protólitos de gnaisses e migmatitos do nordeste do Domínio Carajás teria ocorrido durante o Mesoarqueano, sendo o segundo e último evento de migmatização regional datado em 2859 ± 2 Ma (U-Pb em cristais de zircão de leucossoma indeformado). Delinardo da Silva (2014) descreve a ocorrência de migmatitos na região de Canãa dos Carajás, a sul da bacia de Carajás, e associa eventos anatéticos com o desenvolvimento de um orôgeno no mesoarqueano (3,0-2,93 Ga), possivelmente associado a eventos de granitogênese na região.

Desde os primeiros levantamentos geológicos regionais (Silva *et al*. 1974; Hirata *et al*. 1982; Araújo *et al*. 1988; DOCEGEO, 1988) o Complexo Xingu é reconhecido como uma associação de granitóides e rochas de alto grau metamórfico. Apesar disso, a compreensão de sua evolução geológica durante o Mesoarqueano, prévia à instalação da Bacia Carajás, é ainda limitada e controversa. Nas últimas décadas, poucos trabalhos

objetivaram uma caracterização petrográfica, geoquímica e geocronológica detalhada das rochas metamórficas de alto grau do Complexo Xingu, particularmente na porção nordeste do Domínio Carajás. Nesse contexto, este trabalho se justifica como uma contribuição para o melhor entendimento da evolução geológica de rochas do embasamento do Domínio Carajás durante o Mesoarqueano.

OBJETIVOS

O presente trabalho de mestrado tem como objetivos a:

i. Caracterização geológica dos litotipos pertencentes ao embasamento mesoarqueano (ortognaisses e migmatitos do Complexo Xingu) no nordeste do Domínio Carajás.

ii. Caracterização petrográfica e geoquímica dos ortognaisses e migmatitos;

iii. Delimitação do(s) intervalo(s) de idade de evento(s) anatético(s) na porção nordeste do Domínio Carajás.

MÉTODOS

Trabalho de Campo

O levantamento de campo foi feito em apenas uma etapa de trabalho, com duração de 9 dias, entre os dias 13 e 22 de Julho de 2015, no nordeste da Província Carajás, na região da Serra Leste (no entorno dos municípios de Parauapebas e Curionópolis). Nesse período foram visitados os afloramentos atribuídos ao Complexo Xingu, com destaque às Pedreiras Britamil e Britalider, visando à determinação do modo de ocorrência dos litotipos, relações entre os mesmos, estruturas tectônicas, evidências de fusão parcial e coleta de amostras.

Petrografia

Estudos petrográficos detalhados em luz transmitida e refletida foram desenvolvidos no IG-UNICAMP em lâminas delgadas-polidas confeccionadas a partir de amostras coletadas em campo. Tais estudos permitiram a identificação de evidências de fusão parcial e o estabelecimento das relações entre microestruturas e minerais primários, e sobreposição de eventos tectono-metamórficos e/ou hidrotermais.

Microscopia eletrônica de varredura

Estudos de microscopia eletrônica de varredura (MEV), com destaque à catodoluminescência, realizados no IG-UNICAMP visaram à caracterização detalhada de

fases minerais, zoneamentos composicionais em minerais ígneos e metamórficos, cristalizações secundárias e intercrescimentos.

Geoquímica de Rocha Total e Geocronologia

Todas as etapas laboratoriais foram realizadas nos laboratórios do IG-UNICAMP. As análises em rocha total foram obtidas em espectrômetro de fluorescência de raios X, seguindo os métodos utilizados no laboratório de geoquímica analítica do IG-UNICAMP (Vendemiato & Enzweiler, 2001). Os elementos traço (e.g. La, Nd, Sm, Eu, Yb, Nb, Ta, Zr, Ba, Hf, Th, Sc), foram analisados por ICP-MS, segundo o procedimento descrito em Navarro *et a*l. (2008). Os dados geocronológicos foram obtidos pelo método LA-ICP-MS U-Pb em cristais de zircão no laboratório de geologia isotópica. Os procedimentos analíticos estão descritos detalhadamente no artigo em anexo.

TERMINOLOGIA DE MIGMATITOS EMPREGADA NESSE ESTUDO

A heterogeneidade e singularidade das ocorrências de migmatitos reflete a complexidade evolutiva dessas rochas. Sua diversidade característica deu origem a diferentes terminologias usadas na literatura, muitas vezes confusas devido à consideração tanto de aspectos estruturais, quanto composicionais e genéticos.

A dificuldade do estudo de migmatitos se torna maior quando não há o controle da classificação correta de suas partes constituintes e estruturação. Migmatitos são constituídos de pelo menos duas partes diferentes, necessariamente correlatas, cuja forma de ocorrência varia de acordo com a natureza dos protólitos, taxa de fusão e deformação (Sawyer 2008).

As estruturas anatéticas, ou seja, a forma de ocorrência e relações guardadas entre as partes constituintes de migmatitos, são bem individualizadas e descritas por Sawyer and Brown (2008). Entretanto no que diz respeito à classificação das próprias partes constituintes, algumas divergências ainda são encontradas.

As principais nomenclaturas utilizadas na atualidade são propostas por Vernon (2004) e Sawyer (2008), e ambas consideram a terminologia unificada desenvolvida por Mehnert (1968). Considerando a complementaridade das definições propostas por esses autores, o glossário dos termos empregados neste trabalho para a classificação das partes constituintes de migmatitos é exposto a seguir:

Paleossoma: parte de um migmatito que não sofreu fusão; não necessariamente corresponde ao protolito do migmatito.

Protolito: rocha parental que sofreu fusão, dando origem ao neossoma; fonte de magma (*melt*);

Mesossoma: rocha modificada quimicamente em maior ou menor intensidade durante a anatexia, cuja composição é a mais semelhante à do protólito do migmatito;

Neossoma: constituído por resíduo e leucossoma; produtos neoformados a partir da fusão do protólito;

Leucossoma: porção leucocrática, predominantemente félsica; representa o antigo *melt* cristalizado;

Resíduo: fração sólida deixada após a fusão e extração parcial ou total do magma, inclui fases que não participam das reações de fusão e fases peritéticas; pode ser referido como melanossoma, caso seja melanocrático.

SÍNTESE DOS RESULTADOS

Os resultados da pesquisa desenvolvida são integralmente apresentados no artigo anexo a ser submetido, após o exame de defesa, a periódico internacional a definir.

REFERÊNCIAS

Araújo O.J.B., Maia R.G.N., Jorge-João, X.S. Costa, J.B.S. 1988. A megaestruturação da folha Serra dos Carajás. In: Congresso Latino Americano de Geologia., 7, pp. 324–333.

Delinardo da Silva, M.A., 2014, Metatexitos e diatexitos do Complexo Xingu na região de Canaã dos Carajás: implicações para a evolução mesoarqueana do Domínio Carajás: Unpublished M.Sc. thesis, Campinas, Brazil, Universidade Estadual de Campinas, 100p.

DOCEGEO 1988. Revisão litoestratigráfica da Província Mineral de Carajás – Litoestratigrafia e principais depósitos minerais. 35o Congresso Brasileiro de Geologia, Belém, SBG, Proceedings, 11–54.

Feio, G.R.L., Dall'Agnol, R., Dantas, E.L., Macambira, M.J.B., Santos, J.O.S., Althoff, F.J., Soares, J.E.B. 2013. *Archean granitoid magmatism in the Canaã dos Carajas área: implications for crutal evolution of the Carajás Province, Amazonian Craton, Brazil.* Precambrian Research, 227: 157-185.

Hirata W.K., Rigon J.C., Kadekaru K., Cordeiro A.A.C., Meireles E.A. 1982. Geologia Regional da Província Mineral de Carajás. In: Simp. Geol. Amaz., 1, Belém, SBG/NO, p. 100–110.

Kröner, A., Hegner, E., Wendt, J.I., Byerly, G.R., 1996.*The oldest part of the Barberton granitoid–greenstone terrain, South Africa: evidence for crust formation at 3·5 and 3·7 Ga*. Precambrian Research, v. 78 (pg.105-124)

Machado N., Lindenmayer D.H., Krough T.E., Lindenmayer Z.G. 1991. *U-Pb geochronology of Archean magmatism and basement reactivation in the Carajás area, Amazon Shield, Brazil.* Precambrian Research, 49:329-354

Mehnert, K.R. 1968. *Migmatites and the origin of the granitic rocks*. Elsevier, New York, 393p.

Moreto C.P.N., Monteiro L.V.S., Xavier R.P., Amaral W.S., Santos T.J.S., Juliani C., and Souza Filho C.R. 2011. *Mesoarchean (3.0 and 2.86 Ga) host rocks of the iron oxide-Cu-Au Bacaba deposit, Carajás Mineral Province: U-Pb geochronology and metallogenetic implications*. Mineralium Deposita V. 46, pps. 789-811. doi: 10.1007/s00126-011-0352-9.

Moreto C.P.N., Monteiro L.V.S., Xavier R.P., Creaser R.A., DuFrane A., Melo G.H.C., Delinardo da Silva M.A., Tassinari C.C.G., SATO K. 2014. *Timing of multiple hydrothermal events in the iron oxide copper gold deposits of the Southern Copper Belt, Carajás Province, Brazil.* Mineralium Deposita, v. X, p. 1-30. doi 10.1007/s00126-014-0549-9

Nutman, A.P., Friend, C.R.L., Horie, K., Hidaka, H. 2007. The Itsaq *Complex of southern west Greenland and the construction of Eoarchean crust at convergent plate boundaries*. Developments in Precambrian Geology, 15: 187-217.

Sawyer, E.W. 2008. Atlas of migmatites. Ottawa, The Canadian Mineralogist Special Publication, 9, 371 p.

Sawyer, E. W. and Brown, M., 2008. *Working with Migmatites.* Quebec: Mineralogical Association of Canada.

Sawyer, E.W., Cesare, B., Brown, M. 2011. *When continental crust melts*. Elements, 7: 229-234.

Silva G.G., Lima M.I.C., Andrade A.R.F., Issler R.S., Guimarães G. 1974. Geologia. In: Levantamento de recursos naturais. Projeto Radam: Folha SB.22 Araguaia e pane da Folha SC.22 Tocantins. Rio de Janeiro, MME-DNPM. v. 4, 143 p.

Vendemiatto, M.A., Enzweiler, J., 2001. *Routine control of accuracy in silicate rock analysis by X-ray fluorescence spectrometry*. Geostandards Newsletter The Journal of Geostandards and Geoanalysis 25:283-291.

Vernon, R.H. 2008. *A pratical guide to rock microstructure*. 2nd ed. Cambridge.

ANEXO

ARTIGO: MIGMATITES OF THE XINGU COMPLEX IN THE NORTHEASTERN PART OF THE CARAJÁS DOMAIN, AMAZON CRATON - BRAZIL.

ABSTRACT

This work examines field relationship and petrography of migmatites at the northeastern part of the Carajás Domain, Amazon Craton, and presents new geochemical and geochronological data in order to contribute to understanding the nature and significance of anatexis during the mesoarchean evolution of Carajás Domain. Regionally, in the northeastern Carajás area, the Xingu banded Orthogneiss corresponds to the highest metamorphic-grade rock with minimum leucosome content among the studied litotypes. The mafic layers are clinopyroxene-bearing amphibolite with calcium-rich plagioclase in paragenesis, suggesting at least upper amphibolite facies metamorphism. The migmatites of the Xingu Complex are well exposed in two localities, the Britalider and the Britamil quarries. These migmatites are spatial and temporally related though individually form a complex relationship spectrum from metatexites to diatexites, in which the constituent parts varies according to the source-rock and melting rates. The dominant rock types at the Britalider Quarry are amphibolite and metatonalite to trondhjemite structured as i) patch metatexite; ii) stromatic metatexite; iii) schollen diatexite and iv) schlieren diatexite. The predominant rock types at Britamil quarry are a light-gray tonalite gneiss, a metagranodiorite, and an amphibolite, which are structured as i) stromatic metatexite and ii) nebulitic to schlieren diatexite migmatites. In comparison to the Britalider Quarry, the Britamil migmatite reveals lower melting rates, as amphibolite paleosome remained unmelted during anatexis and melt accumulation as diatexites are less expressive. In the Britamil quarry, a high-temperature event at ca 2.88 Ga is registered in zircon grains of a Hercynite-Cordierite–bearing gneiss, which might represent a retrogressed granulite. The petrological diversity produced in these migmatites occurrences provide examples of how the water content and strain rates are as determinant as the protolith composition and temperature in melting of high-grade rocks. Field relationships and detailed petrography strongly suggest that the Xingu banded Orthogneiss most likely represent a parental gneiss of the Xingu migmatites at Britalider Quarry. The comparison of geochemical igneous fingerprints of the mafic layers of the Xingu banded Orthogneiss and the Britalider quarry amphibolite mesosome is not conclusive, though suggests a petrogenetic link between these units. The Xingu migmatites at Britamil quarry preserve the tonalite gneiss mesosome, suggesting that the metatexite closest protolith was a composite gray gneiss. The Tonalite gneiss mesosome presents severe HREE depletion, high La/Yb ratio and low Y, which indicate a TTG series affinity for its igneous protolith. Emphasis was given to detailed petrography and microstructural analysis, which in addition to whole rock geochemistry and U-Pb zircon geochronology data provide evidence that the Carajás mesoarchean basement rocks underwent partial melting at ca 2.86 Ga.

Keywords: Migmatites, Mesoarchean, Carajás Domain.

INTRODUCTION

The Gneiss-Migmatites complexes represent a significant constituent of Archean terranes (e.g: Superior Province, Sawyer 2008; Itsaq Complex, Nutman et al 2007; Kapvaal Craton, Kröner et al. 1996). Within worldwide cratons, exhumed slices of the lower-crust comprise gray to banded orthogneisses and migmatites. Migmatites are rocks formed by partial melting in great crustal depths and elevated temperatures (>650ºC), similar to conditions developed in mature orogens (Sawyer 1998; 2001, Sawyer et al 2011). Partial melting thus represents the main reworking process to achieve crustal differentiation (Vielzeuf et al. 1990; Brown 1994; 2007; 2013).

Anatexis is a highly sensitive process, which depends on the combination of determinant variables, such as protolith composition (source-rock), metamorphic grade and melting mechanisms. Several authors proposed diverse melting mechanisms and driving forces to accomplish migmatites petrological diversity (i.e. water assisted, fluid absent hydrate-breakdown, deformation enhanced, decompression related; e.g. Hollister and Crawford, 1986; Mogk 1992; Prince et al. 2001; Berger et al. 2007; Sawyer 2010, Song et al. 2014; Zhang et al. 2014; Weinberg and Hasalová 2015; Carvalho et al. 2016). The fluid assisted melting (water influx) associated with regional metamorphism has been largely accepted for numerous migmatites studies (Hasalová et al 2008a, 2008b, Weinberg & Hasalova 2015, Carvalho et al 2016). These studies state that water and stress in addition to heat represent key controls in partial melting.

In the Carajás Domain, which corresponds to the northern part of the Carajás Province, the first descriptions of the mesoarchean basement units grouped undifferentiated rocks, such as gneisses, migmatites, anphibolites and granites, as the Xingu Complex (Silva et al. 1974). Subsequent works (Machado et al. 1991; Vasquez et al. 2008a; Moreto et al. 2011, 2015a; Feio et al., 2012a, 2013, Delinardo da Silva, 2014, Delinardo da Silva et al., 2015; Tavares, 2015) detailed the mode of occurrence, and provided petrography and age constraints of the Xingu Complex assemblage, giving rise to more specific sectioning. Machado et al. (1991) recognized at least two partial melting events at northeastern Carajás Domain, the last one at 2859 ± 2 Ma (U-Pb in zircon grains of undeformed leucosome). The geochronological results presented by these authors were reinterpreted by Barros et al (2010) as granitoids crystallization ages, due to the lack of clear partial melting evidences. Recently, in the southern Carajás Domain (Canaã dos Carajás area), Delinardo da Silva et al (2015) described high metamorphic grade orthopyroxene-bearing gneisses, metatexites and diatexites migmatites, rearising the debate over the partial melting of the Xingu Complex.

In this study, we present new field and microstructural evidences for the partial melting of the Xingu orthogneisses, resulting in the production of migmatites in the northeastern Carajás Domain area. We also provide new geochemical and geochronological data aiming to discuss the migmatites protolith nature and the timing of anatexis.

GEOLOGICAL SETTING OF THE CARAJÁS DOMAIN

The Carajás Province (Santos 2003) is the most ancient crustal segment of Amazonian craton, situated in its southeastern part, northern Brazil (Tassinari and Macambira 1999; 2004) (Fig. 1A). A crustal discontinuity recognized as a regional E-W direction shear zone divides the province into two tectonic domains: the southern Rio Maria, a typical granite-greenstone terrane of mesoarchean age (Almeida et al. 2010) and the northern Carajás (Vasquez et al. 2008) (Fig. 1B). In its northeastern segment, the Carajás Domain is limited to the north by the Paleoproterozoic Bacajá Domain and to the east by the Neoproterozoic Araguaia Belt (Santos et al. 2000; Santos 2003; Vasquez et al. 2008) (Fig. 1C).

The Carajás Domain is composed of mesoarchean basement rocks, neoarchean intrusive (e.g.: Serra do Rabo, Estrela, and Planalto suites; Barros et al. 2004; Sardinha et al 2006, Feio et al. 2012, 2013) and low-grade metamorphosed supracrustal units; and Paleoproterozoic intrusive A-type granites (e.g.: Central de Carajás, Cigano, and Pojuca; Machado et al. 1991).

The mesoarchean basement rocks are grouped in: i) Pium Complex and Chicrim-Cateté Orthogranulite (Ricci and Carvalho 2006; Vasquez et al. 2008), formely grouped in Pium Complex (Araújo and Maia 1991; Pidgeon et al 2000), ii) Granitoid rocks of TTG and calk-alkaline affinity (Moreto et al. 2011; 2015a; Feio et al. 2013) and iii) Xingu Complex (Silva et al. 1974; Docegeo 1988).

The Pium Complex was first described as an association of mafic and felsic granulites, which yielded a crystallization age of 3,002±14 Ma and granulite-facies metamorphism at 2,859±9 Ma (U-Pb in Zircon; Pidgeon et al. 2000). These ages were later ascribed to the igneous protolith of the Chicrim-Cateté Orthogranulite, a high-grade metamorphic association of charnockite to enderbite rocks, claimed to occur also as enclaves (Ricci and Carvalho 2006; Vasquez et al. 2008) in the Diopside Norite Pium (Ricci and Carvalho 2006). This younger unit (ca. 2.7 Ga) (Santos et al. 2013c) comprises gabbroic rocks of the charnockitic series found at the Pium river type locality.

The mesoarchean rocks of TTG and calk alkaline affinity are isotropic to foliated or homogenous to banded, biotite-hornblende bearing granitoids (Moreto et al. 2011, 2015a,

2015b Feio et al. 2012, 2013). These granitoids correspond to Bacaba Tonalite and Sequeirinho granite (ca. 3.0 Ga; Moreto et al. 2011; Moreto et al. 2015b); Canaã dos Carajás granite (ca. 2.96 Ga) (Feio et al. 2013); Serra Dourada, Cruzadão and Bom Jesus granites, Rio Verde Trondhjemite and Campina Verde Tonalite (ca. 2.87 to 2.83 Ga) (Moreto et al. 2011; Feio et al. 2013; Moreto et al. 2015b).

The Xingu Complex outcrops more expressively at the southern Carajás Domain (Fig.1c). In the Canãa dos Carajás area, the Xingu Complex comprises patch and stromatic metatexites, schlieren and schollen diatexites (Delinardo da Silva 2014; Delinardo da Silva et al. 2015). The paleosome part consists of diopside-hornblende orthogneiss (mafic gneiss) and quartz amphibolite enclaves or lenses. The mainly tonalitic leucosome is hosted by orthopyroxene-diopside gneisses. Zircon grains of a deformed leucosome yielded an upper intercept crystallization age of 2959 ± 15 Ma (U-Pb SHRIMP zircon), interpreted as an anatectic event related to regional metamorphism (Delinardo da Silva 2014; Delinardo da Silva et al. 2015).

In the northeastern part of the Carajás Domain (Serra Leste area), Machado et al. (1991) identified at least two migmatisation events by field crosscutting relationships observed at the Britamil Quarry (Fig. 1D), formerly known as Cimcop Quarry. For those authors, the last high-grade metamorphic event accompanied by anatexis took place at 2859 ± 2 Ma, coeval to Pium Complex granulite facies metamorphism. Barros et al (2010) instead interpreted these ages as related to granitoid rocks crystallization, arguing the lack of clear migmatites structures. Those authors describe rocks of tonalite, trondhjemite and quartz diorite composition, which display sub-vertical primary magmatic foliation with the presence of amphibolite xenoliths.

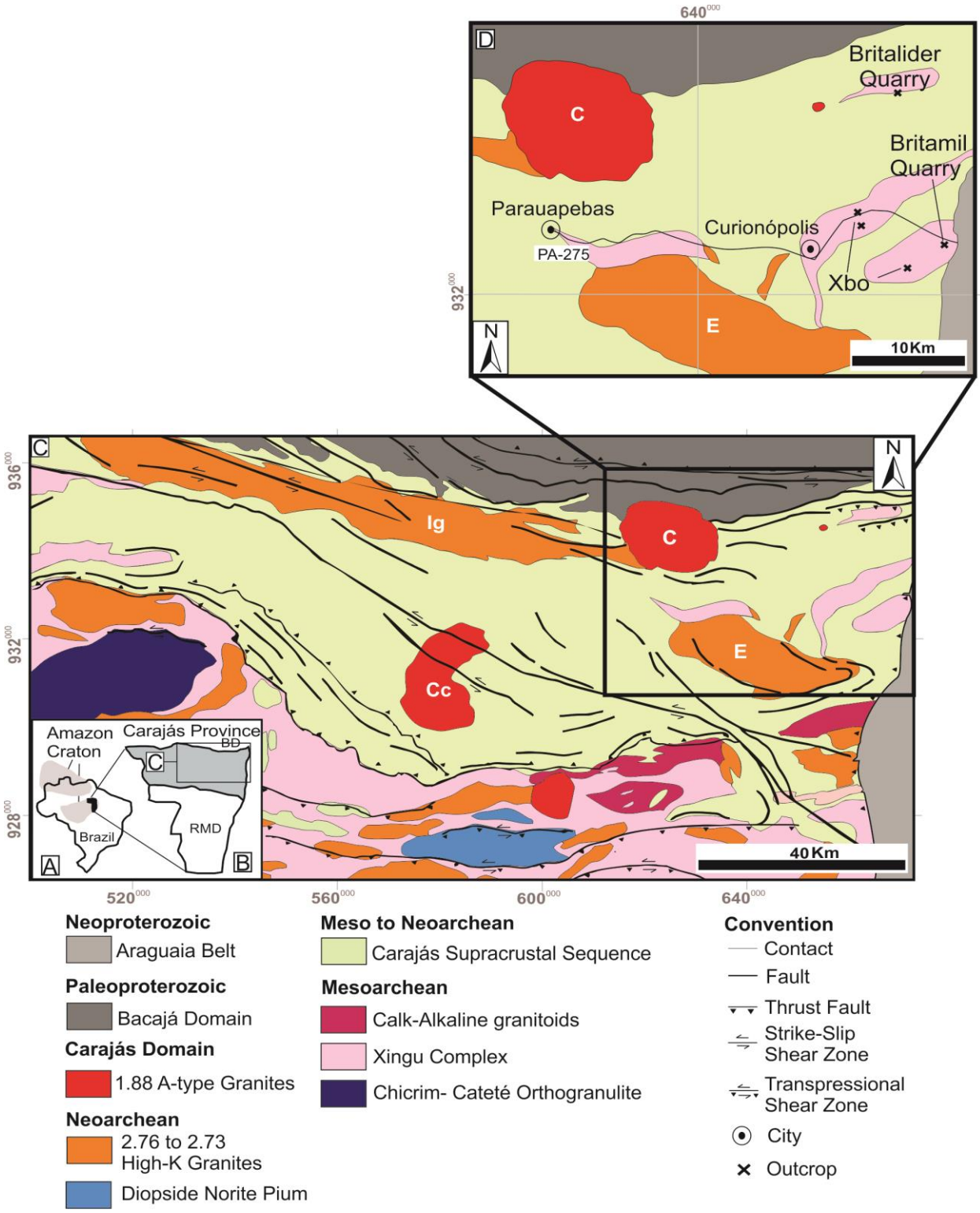

Fig. 1: Geological Map of the Carajás Domain (compilation of Vasquez et al 2008; Tavares 2015). A) Location in Brazil; B) Carajás Province in Amazon Craton (BD Bacajá Domain, RMD Rio Maria Domain); C) Geological Map of the Carajás Domain (C: Cigano, Cc: Central de Carajás, Ig: Igarapé Gelado, E: Estrela; D) Sketch map of the studied area, showing Britalider and Britamil quarries and the surrounding outcrops (Xbo: Xingu banded orthogneiss)

ANALYTICAL PROCEDURES

Sampling carried during fieldtrip prioritized rocks more preserved from hydrothermal alteration. Sample preparation, and the geochemical and geochronological analyses were made at the Institute of Geoscience of the State University of Campinas (UNICAMP). Nineteen representative samples of diverse lithotypes were selected for whole-rock geochemistry. From 0.5 to 1.0 kg of rock samples were crushed and then powdered using both rings and planetary agate mills. Major elements were determined by XRF performed at the Geochemistry Laboratory following the method proposed by Vendemiatto & Enzweiller (2001), using a Philips PW2404 X-Ray fluorescence spectrometer. Trace elements were measured by ICP-MS at the Isotope Geology Laboratory as described by Navarro et al. (2008), using an Inductively Coupled Plasma-Mass Spectrometer X series II (Thermo) equipped with a Collision Cell Technology (CCT). Geochemical data calculations and diagrams were handled by GCDKit free software (version 4.1; Janousek et al. 2006).

A set of four samples were selected for zircon U-Pb LA-ICP-MS geochronology. Samples were crushed and ground in a jaw crusher. Heavy minerals, including zircon, were concentrated using conventional gravity and magnetic techniques. The least magnetic zircon grains were hand-picked under a binocular microscope, mounted in epoxy blocks and polished for exposing central sections. Cathodoluminescence (CL) and Secondary electron (SE) imaging were performed for grain analysis and targeting. CL conditions were: accelerating voltage 15kV, work distance of 16mm and emission current varying from 3000pA to 8000pA. The analyses were carried at Isotope Geology Laboratory using a Thermo Fisher Element XR sector field ICP-MS and a Photon Machine Excite 193nm ultra-short pulse excimer laser ablation system (Analyte Excite WH) with a HelEx 2 volume cell. Laser conditions were: spot size of 25µm, frequency of 10 Hz, and laser fluence of 4.7 J/cm2. Zircon grains did not contain common Pb, implying no need for correction. Concordia ages and diagrams were obtained through reduction using IOLITE software (2.5 version-laboratory license).

XINGU GNEISSES AND MIGMATITES

Outcrops of the basement units are scarce in northeastern Carajás. According to Tavares (2015), the Xingu Complex occur as lenses in tectonic contact with supracrustal units by reverse shear zones (Fig. 1C; Tavares 2015). The two best expositions of the Xingu Complex are located at the Britalider and the Britamil (former CIMCOP) quarries (Fig 1D). The high metamorphic grade rocks recognized in this study at these localities show substantial evidence for partial melting with a variety of leucosome styles. The highest-grade

rocks without or with minimum leucosome are banded orthogneisses found in a few surrounding outcrops (Fig. 1D). In order to refer to individual rock types, this study employs the migmatite terminology of Sawyer and Brown (2008) and Vernon (2008).

Xingu Banded Orthogneiss

The banded orthogneiss occurs as in situ meter-scale blocks of interlayered felsic and mafic foliated bands (Fig.2A). The mafic bands correspond to medium- to coarse-grained amphibolite, in which mineral paragenesis is hornblende + plagioclase (labradorite) + titanite ± diopside ± rutile ±epidote. Common accessory minerals are apatite, zircon, ilmenite, magnetite and pyrite. The predominant texture is granoblastic, defining a polygonal microstructure, though disequilibrium grain boundaries, such as curved contacts or small apparent dihedral angles, are also common (Fig 2 B,C,D). Films of quartz and plagioclase in a cuspate shape or with rounded tips occur at grains junctions (Fig. 2B,D).

The felsic bands are composed of coarse-grained quartz and plagioclase with accessory zircon. Minor amounts of xenomorphic to subidiomorphic hornblende, titanite, rutile and epidote are present in the transition between bands. This transitional layer presents an abrupt grainsize reduction and distinctive rounded to lobate grain shapes (Figs. 2E,F,G,H). Centimeter-scale leucocratic veins, composed of plagioclase and quartz and surrounded by amphibole megacrysts, crosscut the banded orthogneiss.

Migmatites of the Britalider Quarry

The dominant rock types at the Britalider Quarry are mesocratic amphibolite and leucocratic metatonalite to trondhjemite structured as a transitional spectrum of migmatites (Fig. 3A). The morphologies recognized at the quarry are i) patch metatexite; ii) stromatic metatexite; iii) schollen diatexite and iv) schlieren diatexite. The migmatite constituent parts identified correspond to the amphibolite mesosome, *in situ* unsegregated and segregated neosome, *in source* leucosome, mafic residue and leucocratic veins.

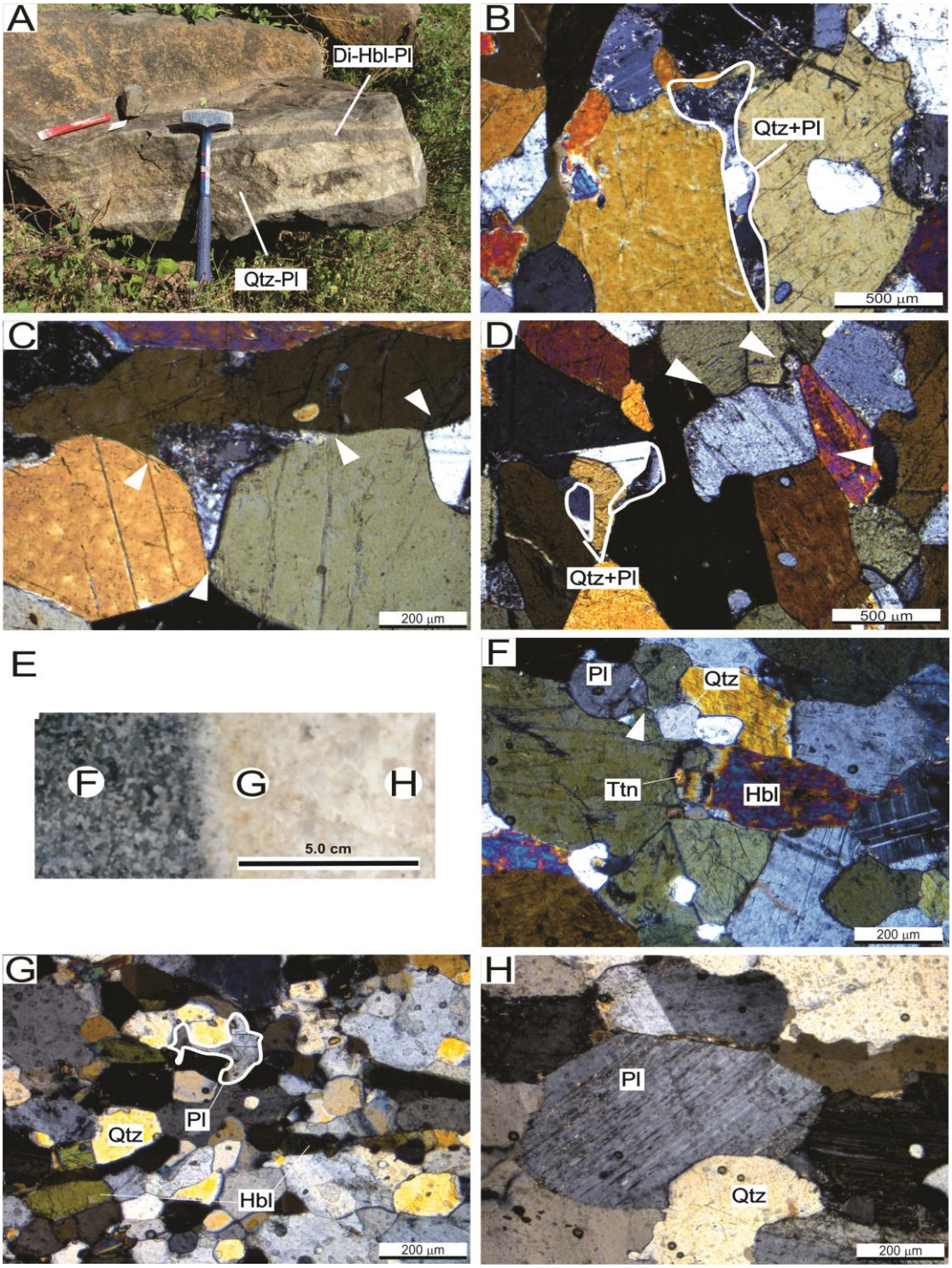

Fig. 2*:* Field aspects and photomicrographs of the Xingu banded orthogneiss. A) Blocks of Xingu banded orthogneiss; B) Xenomorphic plagioclase (Pl) and quartz (Qtz) at a hornblende-hornblende-plagioclase (Hbl-Pl) cuspate junction, as melt pseudomorphous; C) Hbl–Pl cuspate grain boundaries. The top right arrow indicates a larger dihedral angle. D) Xenomorphic plagioclase and quartz as melt pseudomorphous. The top left arrow indicates a high angle (~180º) at Hbl-Pl junction, the bottom arrow, a smaller dihedral angle (~60º); E) Hand specimen showing the transition from mafic to felsic layer of banded orthogneiss; F) mafic layer, with rounded plagioclase+quartz grains; G) Transitional layer, showing, grain size reduction with plagioclase highly lobate shapes; H) felsic layer, showing grain size coarsening. Photomicrographs were taken under crossed polarizers.

Metatexites and Diatexites

The metatexite migmatites are a small part of the quarry that preserve compositional layering, structured analogously to the banded orthogneiss. Stromatic metatexite presents centimeter- to meter-scale mafic mesosome layers interbedded with leucosome sheets (Fig.3A). The amphibolite mesosome contain several patches of unsegregated *in situ* neosome, constituted by quartz-plagioclase leucosome and amphibole megacrysts (Fig. 3B), interpreted here as perithetic phases. Lenses and patches of segregated in situ (Fig 3C) and in source (Fig 3E leucosome occur within the mesosome layers, and these structures may eventually display rims of mafic selvage (Fig. 3D).

Expressive volume of neosome occur as diatexites. Diatexites are leuco- to hololeucocratic, medium- to coarse-grained, protomylonitic rocks of tonalitic composition. These rocks are heterogeneous concerning the percentage of residue and structures, with abrupt variations producing petrological diversity through schlieren to more homogenous diatexites (Figs. 3F to H). The orientation of hornblende and biotite evidence a foliated fabric in schlieren diatexite. The schlieren are either continuous or discontinuous and predominantly narrow (up to 1 cm), though wider (up to 8cm) concentrations are also present (Fig 3G).

Mesosome fragments occur in the schlieren and homogeneous diatexites, defining a schollen structure. These are centimeter- to meter-scale, sub-rounded to highly stretched blocks and rafts of amphibolite mesosome, which are sub-parallel to schlieren foliation. Mesosome boudinage within leucosome layers occurs as former melt content increase, marking the transition from stromatic metatexite to schollen diatexite (Fig 3A). The mesosome boudins are meter scale and weakly asymmetrical, disposed in a low angle anastomosed foliation between 30/40 and 180/25. The leucosome is either concordant to boudins or discordant, filling boudins necks at disruption sites (Fig.3A). Intrusive sub-parallel leucocratic veins, mainly composed of plagioclase and quartz, and with mafic residual lenses and selvage crosscut diatexite bodies (Fig. 3I). These leucocratic veins are similar to those crosscutting the Xingu banded orthogneiss that outcrop in the quarries surroundings.

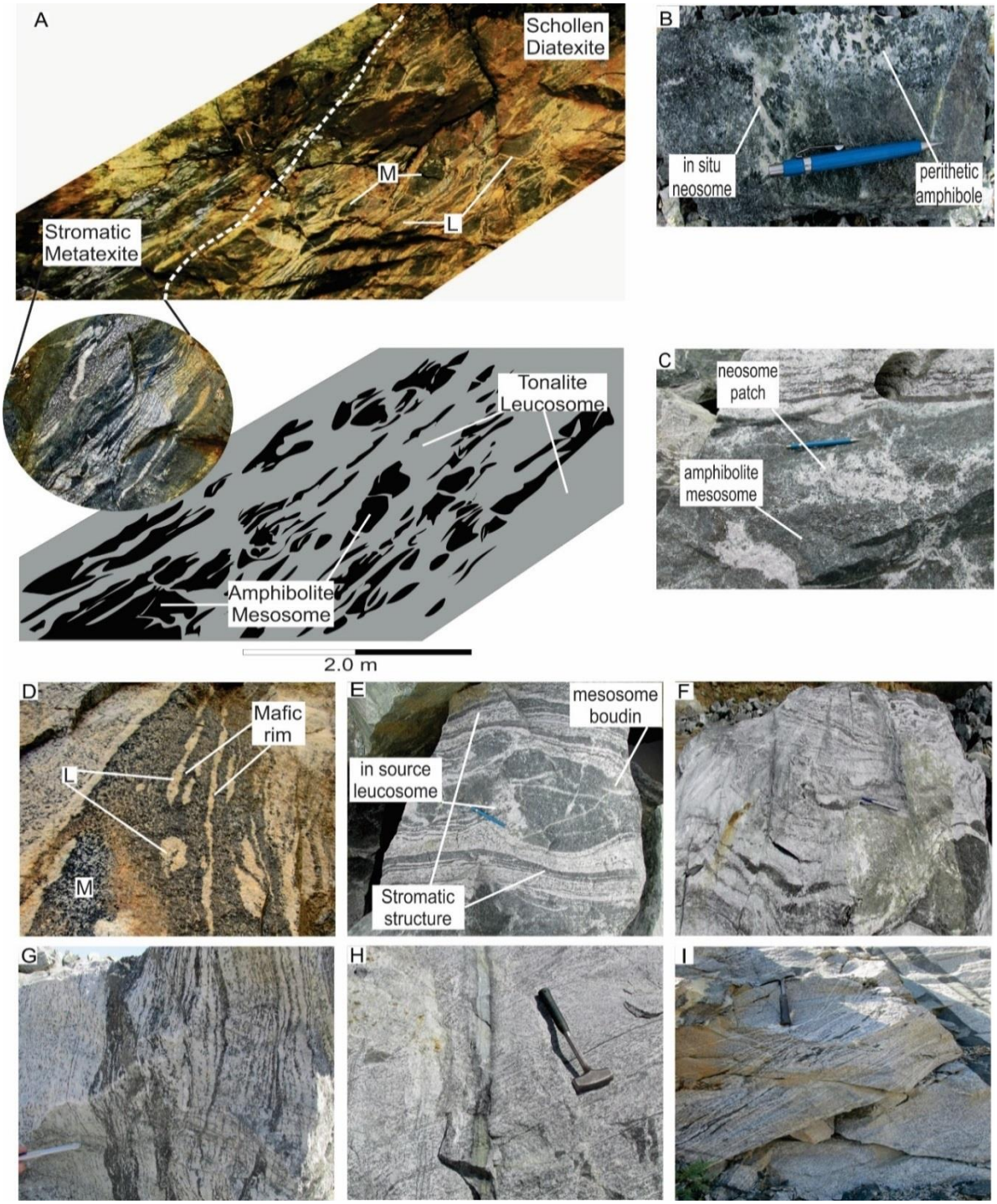

Fig. 3: Field aspects of the Xingu migmatite at the Britalider quarry A) Photo and scheme of thick layered stromatic metatexite (left) evolving to schollen diatexite with boudinage of the mesosome (M) (right). Detail of the crosscutting and parallel to foliation leucosome (L), B) in situ leucosome with amphibole megacryst, C) in situ neosome patches within amphibolite mesosome raft, D) trondhjemitic leucosome tortuous forms, bordered by mafic residue in an amphibolite layer, E) metatexite to diatexite transition, showing in source leucosome within the amphibolite mesosome boudin parallel to stromatic structures, F) Diatexite displaying schollen, schlieren and homogeneous facies, G) metatrondhjemite (left) to metatonalite (right) diatexite, showing abrupt variation in schlieren content and (right) continuous, H) schlieren phantoms of foliation in a metatonalite diatexite, I) leucocratic veins with mafic residual lenses cutting across homogeneous metatronhjemite diatexite.

The original gneissic metamorphic foliation is preserved as stromatic structure (Fig 4A) in the metatexites and within the amphibolite mesosome boudins, defined by hornblende alignment, as detailed in the next section. The Sn foliation shows incipient folding in stromatic metatexites (Fig. 4B), developing ductile structures typical of deep crustal levels. Mafic schlieren in diatexites define a second foliation (Sn+1) sub parallel to the Sn foliation (Fig 4C). A third foliation (Sn+2) crosscut and locally transposes both Sn and Sn+1. The Sn+2 mylonitic foliation is spaced and obliterates migmatites structures (Figs. 4A to C) due to shearing during transition to shallower crustal levels.

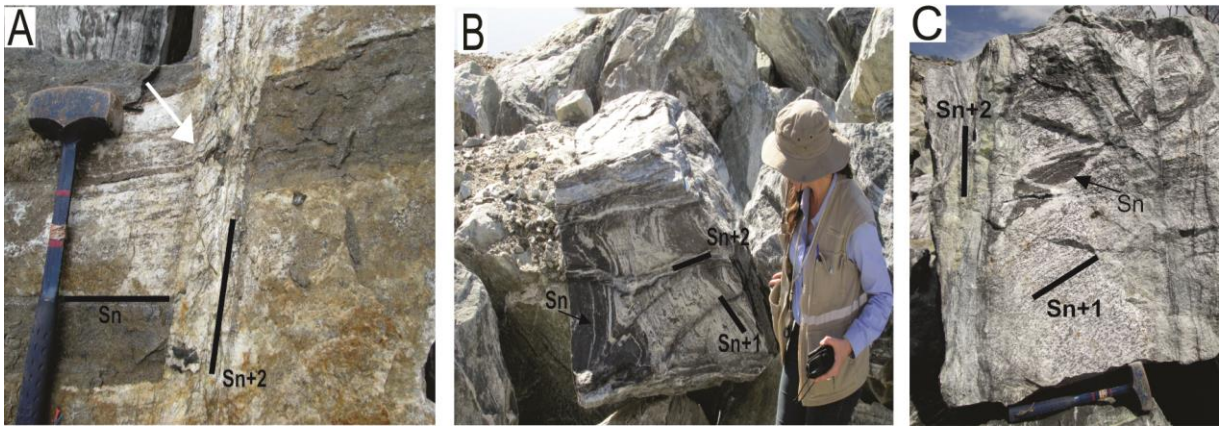

Fig. 4: Deformational structures of the Xingu migmatite at Britalider quarry A) Stromatic metatexite exhibiting Sn gneissic foliation (parallel to compositional banding), transposed by Sn+2 (mylonitic foliation); B) Incipient folding of the stromatic structure in a metatexite; C) stretched amphibolite mesosome schollen in schlieren diatexite (Sn+1), showing foliation transposing (Sn+2).

Migmatites constituent parts

Regarding the migmatites constituent parts, the mesosome represent the most similar rock to the protolith composition, with chemical modifications achieved during anatexis (Vernon 2008). The Britalider quarry migmatite mesosome corresponds to mesocratic, greenish, medium- to coarse-grained amphibolite mainly composed of hornblende and plagioclase, with minor epidote, apatite, titanite and magnetite. The hornblende porfiroclasts are predominantly sub-idiomorphic (Fig. 5A), present corroded shapes, and define a spaced anastomosing mylonitic foliation with granonematoblastic texture locally preserved (Fig. 5B). Plagioclase is labradorite and occurs in a variety of shapes as equant to high-aspect ratio; sigma shaped and rotated sub-rounded grains, which either lack or show deformation twinning with tapering edges and undulose extinction, rarely with carlsbad twinning.

The neosome part of Britalider quarry migmatite is composed of tonalite leucosome, perithetic hornblende megacrysts and residual melanosome. The mafic residue occurs as schlieric melanosome mainly composed of green hornblende and biotite, with minor plagioclase, quartz and epidote (Fig. 5C). Biotite presents uncommon pseudo-hexagonal sections hence interpreted as possible hornblende pseudomorph (Fig. 5D). The schlieren crystal aggregates show either a strong preferred orientation (Figs 5C, D) or randomness (Fig. 5E), as more advanced disaggregation stage develops a flow microstructure. Within the schlieren, hornblende-quartz intergrowth form relict sub-idiomorphic porphyroblasts (Fig 5F).

The leucosome major constituents are plagioclase and quartz with accessory apatite, ilmenite, magnetite, zircon, epidote and allanite. The leucosome shows grain size increase when compared to mesosome and melanosome. Leucosome display mylonitic fabric as evidenced by highly lobate to sutured contacts between quartz-quartz/quartz-plagioclase (Fig 5G), and by coarser-grained quartz with chessboard extinction mantled by medium-grained polygonal quartz aggregates (Fig. 5I). Plagioclase occurs as sub-idiomorphic to xenomorphic, corroded crystals, forming a groundmass, often with obliterated crystal faces (Fig. 5C, D, H). Plagioclase is also present as rounded inclusions in quartz and plagioclase crystals. The leucosome is plagioclase-rich nearby schlieren domains (Figs. 5C, D). Fine-grained quartz and flake-like biotite aggregates fills intergranular spaces in some homogeneous portions of the diatexites, forming veins and pockets, sometimes resembling a cluster texture.

The original composition of the amphibole megacrysts present in the neossome was not determined due to replacement by xenomorphic actinolite. Despite that, field relationship suggests a perithetic origin as these megacrysts occur within in situ leucosome in the metatexite migmatite.

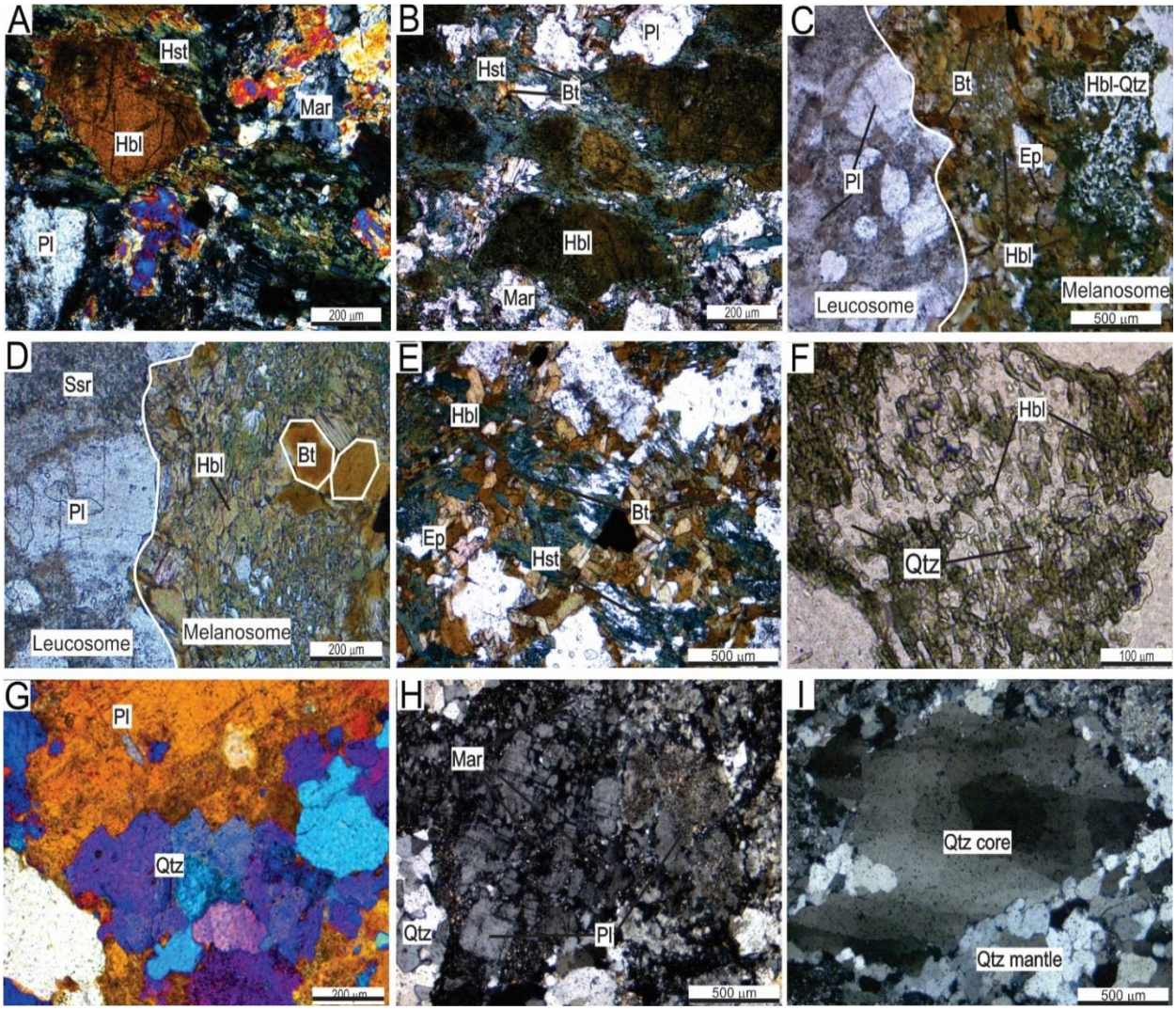

Fig. 5: Microstructures of the mesosome and neosome of the Britalider Quarry Migmatite. Photomicrographs of: the Amphibolite mesosome showing: A) typical microstructure and mineral assemblage under crossed polars B) hornblende (Hbl) porfiroclasts rimmed by hastingsite (Hst) (parallel polars). Photomicrographs of the melanosome and leucosome boundary in the schlieren diatexites showing: C) typical structure and mineral assemblage, D) biotite (Bt) pseudohexagonal sections, E) fine grained clusters of biotite (Bt) and hornblende (Hbl) showing randomness; F) detail of the quartz-hornblende simplectite-like intergrowth. Photomicrographs of the Homogeneous Diatexite showing: G) Stepped sutured contact between quartz (Qtz)-plagioclase (Pl), H) Plagioclase (Pl) intense replacement by marialite (Mar), with gypsum wedge; I) core and mantle quartz microstructure.

Hydrothermal alteration can be conspicuous in the Britalider quarry area, and even more preserved samples presents some level of late stage alteration associated with brittle-ductile shear zones due to mid-crust reworking (Sn+2 foliation). Common late stage features crosscutting the migmatites are: i) mafic dykes with sharp contacts (Fig 3I); and ii) hydrothermal scapolite and pyrite-epidote-quartz veins associated with brittle fault planes, as well as massive actinolite-rich bodies. These altered rocks are characterized by a diversity of replacement textures and retrograde overprints on metamorphic-peak mineral assemblage. Subordinate mineral phases are hastingsite, biotite, quartz, clinochlore and chamosite.

Hastingsite occurs as rims of hornblende grains, replacing plagioclase, as interstitial xenomorphic grains or filling cracks. Scapolite is present as Ca-rich (meionite) and Na-rich (marialite) members. Meionite occurs as an anhedral framework in the matrix (Fig. 5A); and marialite is present in veinlets and commonly replaces plagioclase (Fig.5H). Actinolite is present in the matrix of more altered samples as fine- to medium-grained prismatic crystals. Biotite occurs as elongated subidiomorphic to xenomorphic crystals along cleavage planes in plagioclase, as well as in pressure shadows in hornblende-mantled porfiroclasts. It is always present in amphibole/plagioclase contacts and commonly replaces hastingsite. Quartz is scarce and occurs in the matrix as polygonal fine-grained aggregates, or as ribbon-like discordant veinlets associated with hastingsite-marialite and epidote-clinochlore- chamosite. Clinochlore also replaces biotite. Saussuritization of plagioclase is intense in all samples.

Migmatites of the Britamil Quarry

The predominant rock types at Britamil quarry are a light-gray tonalite gneiss, a metagranodiorite, and a mesocratic amphibolite, which are structured as stromatic metatexite and nebulitic to schlieren diatexite migmatites (Fig 6A). The migmatites constituent parts correspond to: i) tonalite gneiss mesosome; ii) amphibolite paleosome; iii) metagranodiorite leucosome iv) pink granite leucosome and iv) biotite melanosome.

Metatexites and diatexites

The stromatic metatexite is characterized by: i) intercalation of the paleosome and neosome layers (Fig 6A) and ii) centimeter-scale layered leucosome-mesosome pairs with discrete melanosome (Fig 6B). The metatexite migmatite preserve a high-angle to sub-vertical schistose foliation (between 50/80 and 20/80), marked by preferred orientation of biotite. The paleosome amphibolite occurs as layers interbedded within the metatexite, which are foliation parallel and variably injected by leucosome (Fig 6B).

The transition between metatexites and diatexites at the quarry are either abrupt or diffuse. Structures such as gneissic foliation and compositional banding progressively disappear, developing nebulitic diatexites. The granodiorite composition diatexite locally contain thin and continuous schlieric melanosome composed of biotite (Fig 6D), sometimes resembling foliated granitoids.

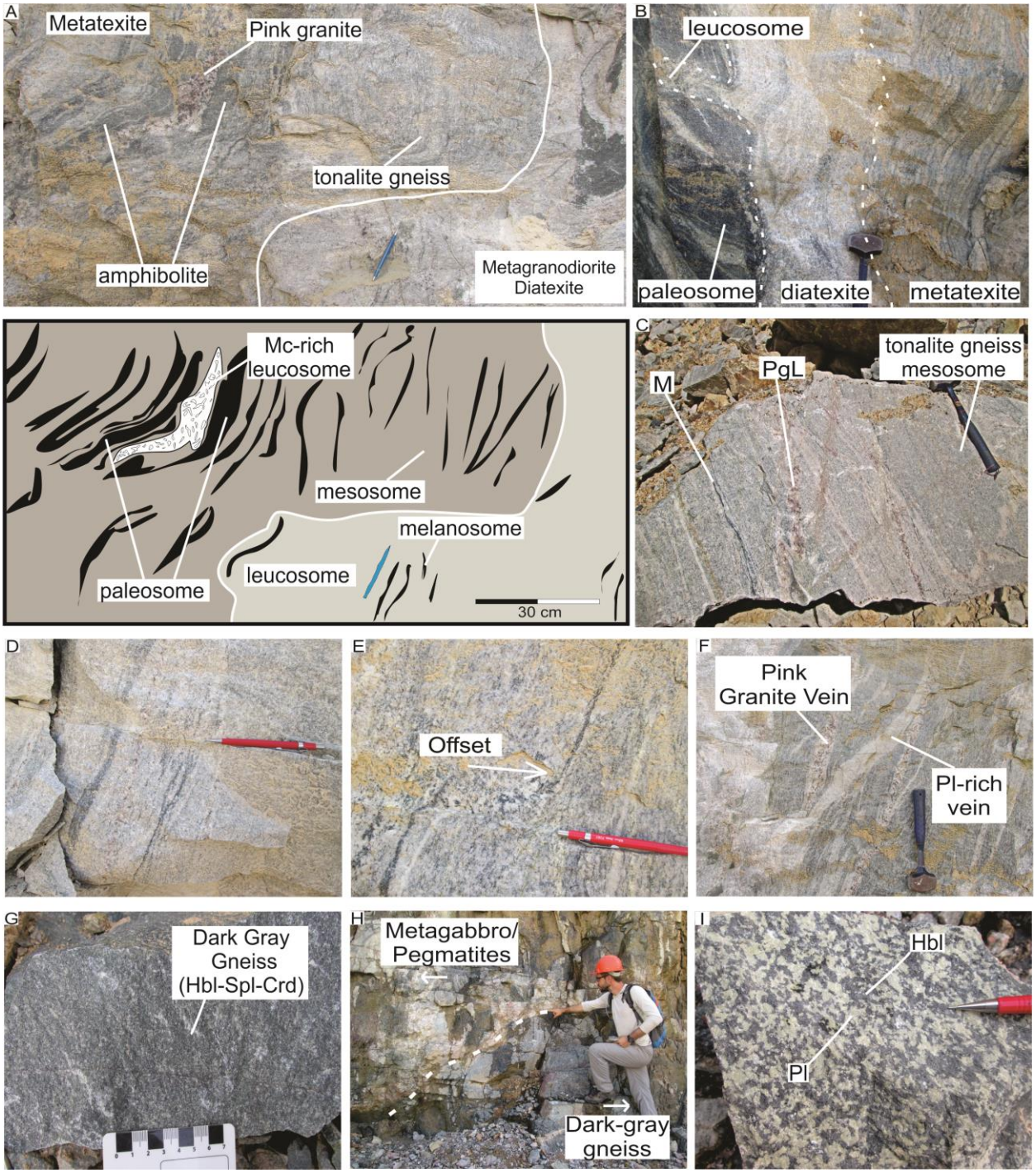

Fig. 6. Field Aspects of the Xingu Migmatites at the Britamil Quarry. A) Photo and scheme showing metatexite to diatexite transition with migmatites main constituent parts: amphibolite paleosome, tonalite gneiss mesosome, pink granite pegmatoid-like leucosome lens and metagranodiorite leucosome as a nebulitic diatexite, with local mafic schlieren ghosts, B) from right to left: gneissic foliation dissapearance in a metatexite to diatexite transition, showing also leucosome injection in the amphibolite paleosome, C) pink granite leucosome (PgL) vein crosscutting the metatexite with locally developed mafic schlieren (M), D) mafic schlieren in a foliated diatexite; E) neosome with diffuse borders filling a foliation offset, F) Pink-coloured coarse grained granitic and plagioclase-rich leucossome veins cutting the migmatite, G) Dark gray gneiss homogeneous appearance; H) Pegmtites marking the transition between the Dark gray gneiss and metagabbro, I) Coarse-grained metagabbro displaying blastosubophitic texture

Locally, millimeter-scale leucocratic patches are observed within shear bands truncating gneissic foliation (Fig 6E). In source leucosome is also present as gray leucocratic fine-grained plagioclase-rich veins and pink coarse-grained microcline-rich veins and lenses, here referred as pink granite (Fig. 6F). Both the plagioclase-rich and the pink granite leucosome varieties occur parallel to foliation or crosscut the metatexite and diatexite as sinuous veins of straight and sharp boundaries. The crosscutting relationship between the two compositionally different leucosomes is ambiguous.

Migmatites constituent parts

The paleosome amphibolite is composed of hornblende and plagioclase arranged in a granonematoblastic texture. Minor chamosite and epidote define a discontinuous and spaced schistosity sub- parallel to hornblende-plagioclase alignment (Fig. 7G). The chlorite-epidote retrograde schistosity is also observed in the tonalite gneiss mesosome.

The tonalite gneiss mesosome is mainly composed of medium-grained plagioclase andesine and quartz with minor microcline, albite and chamosite. Subordinate phases are magnetite, zircon and allanite. Plagioclase and quartz form a polygonal framework with a discontinuous and spaced schistosity marked by chamosite after relicts of biotite. The mesosome constitutes domains where the granoblastic structure is predominant and incipient melting microstructures are preserved (Fig. 7A, B). Equant amounts of plagioclase and quartz form the framework. Interstitial xenomorphic microcline or microcline-plagioclase occur at plagioclase-plagioclase or plagioclase-quartz junctions (Fig. 7C). Highly lobate microcline crystals fill pores, form films and develop microscopic-scale interconnected channels, hence interpreted as former melt pseudomorphous (Fig. 7D).

The plagioclase-rich leucosome domains are mainly composed of plagioclase, microcline and quartz. These domains display an evident grain size increase (1 to 2.5mm) in comparison to mesosome and paleosome (Fig 7E). Though deformed, leucosome preserves igneous features. Quartz grains are mostly irregularly shaped and present undulose extinction and sub-grains texture, whereas rare subidiomorphic grains show crystal faces against plagioclase. Plagioclase occurs as high-aspect ratio well-developed grains. Microcline crystals become larger, coating sub-rounded mymerkyte grains as inclusions, which are also present in the rock matrix.

Pink granite veins and lenses are composed of variable contents of microcline, plagioclase and quartz with accessory titanite, apatite, zircon, rutile. This coarse-grained to pegmatitic rock microstructure is an arrangement of xenomorphic larger crystals of

microcline within a polygonal fine-grained matrix (Fig. 7F). The microcline crystals present undulose extinction and occurs as pools, which envelope thinner microcline, beads of quartz and plagioclase grains. Flame perthite feldspar and plagioclase are found only in the matrix. Quartz is present both in the matrix as well as coarse-grained grains with undulose extinction and incipient sub-grain texture.

Dark gray gneiss

A small body of a dark gray mesocratic gneiss (Fig 6G) occurs in the quarry and its field relationship with the migmatites unit is unclear, though it keeps a contact with a metagabbro voluminous body marked by pegmatitic microcline-rich veins (Fig. 6H). The dark gray gneiss correspond to a medium-grained, homogeneous granoblastic rock, which display a weakly developed foliation, only recognized under the microscope. Major phases are plagioclase, cordierite, dark green hercynite spinel, hornblende and quartz (Fig. 7H), with subordinate chlorite, actinolite, apatite, chlorapatite, epidote, zircon, titanite, ilmenite, magnetite-rutile-titanite intergrowth, chalcopyrite, pyrite and allanite. The plagioclase forms a framework of sub-idiomorphic grains exhibiting polysynthetic, carlsbad or no twinning. Plagioclase also occurs as idiomorphic inclusions in spinel or highly stretched xenomorphic crystals, partially digested by quartz. Cordierite idiomorphic porphyroblasts presents polysynthetic twinning, are arser than plagioclase and are often pinitized. The dark green spinel subidiomorphic crystals display straight contact with cordierite (Fig.7I), plagioclase and hornblende and are often replaced by chlorite and calcite. Green hornblende crystals contain needles inclusions of magnetite and present corroded borders by quartz beads, developing a buldging microstructure (Fig. 7J). Quartz also occurs as large xenomorphic crystals with undulose extinction, commonly isolated by plagioclase framework. Microscopic-scale pockets and thin films composed of quartz and plagioclase or only plagioclase with cuspate boundaries are rarely observed at grain junctions (Fig 7K).

Metagabbro and Pegmatites

The metagabbro occurs as a large body spatially close to the dark gray gneiss. The metagabbro is composed of very coarse-grained hornblende and plagioclase, arranged in a blastosub-ophitic texture and locally foliated due to shearing (Figs. 6I, 7L). Light-pink colored, microcline-rich, pegmatite veins crosscut the metagabbro. The presence of amphibole megacrysts in those pegmatite veins suggest the partial digestion of the metagabbro by the former.

Late epidotization and potassic alteration with potassium feldspar are outspread in the quarry occurring as veins and veinlets systems, filling fracture planes, and developing alteration halos.

WHOLE ROCK GEOCHEMISTRY

This section presents geochemical data of diverse lithologies found in the studied area. We grouped the mafic layers of the Xingu Orthogneiss (3 samples) and the Amphibolite mesosome from Britalider quarry (6 samples) as mafic rocks sub-section. The Britamil quarry lithotypes are described in another sub-section, which includes the Tonalite gneiss mesosome (7 samples), the Pink granite (4 samples) and the Dark-gray Gneiss (1 sample). In order to better understand the geological significance of the felsic rocks geochemical signatures, we present previous studies data (Feio et al. 2012; Delinardo da Silva et al. 2015) from granitoids and migmatites of the southern part of the Carajás Domain. We apply just immobile element geochemistry for the Dark Gray Gneiss as it is a single sample and precludes elements mobility evaluation. Bulk rock compositions are listed in tables 1 and 2.

Major and trace elements of mafic rocks

Regarding the major elements content, the mafic bands of the Xingu Orthogneiss and amphibolite mesosome samples range within a similar interval. The SiO_2 content varies from 46 to 51 wt%, Al_2O_3 from 13.1 to 16 wt. % and CaO from 8.9 to 11.2 wt%. Exceptions are K_2O and LOI values, both lower in the Xingu Orthogneiss compared to the mesosome (table 1). The Magnesium number (Mg#=MgO/MgO+FeOt) varies from 0.37 to 0.53. Variation diagrams of Mg# against major elements display an almost vertical array, suggesting an intense mobilization of major oxides (Figs. 8A to D).

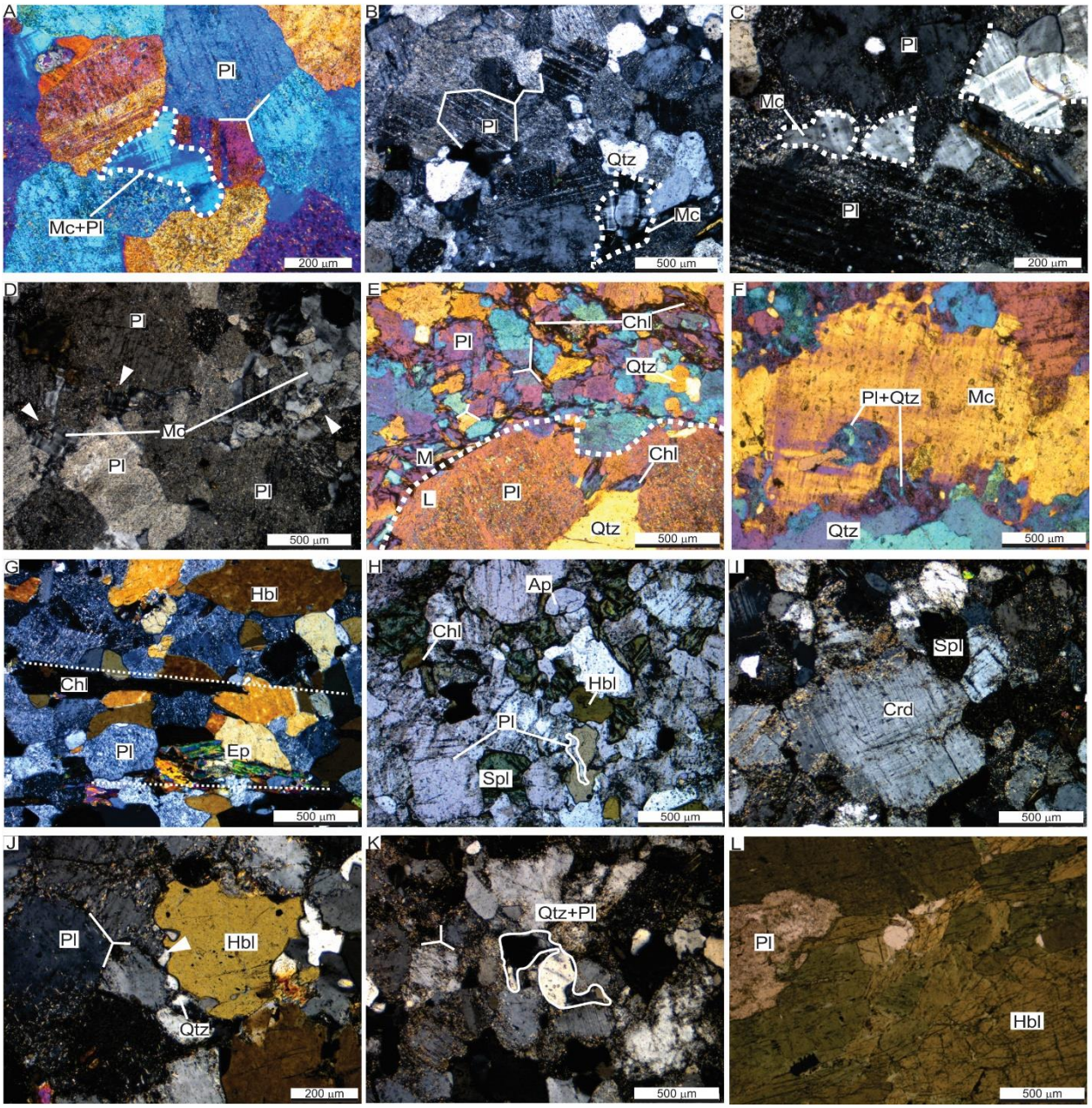

Fig. 7: Photomicrographs of the: Tonalite gneiss mesosome A) granoblastic structure with microcline-plagioclase cuspate grain at plagioclase triple junction, B) and C) fine grained microcline lobate shaped aggregates, as former melt pseudomorphous, D) interstial xenomorphic microcline, resembling former melt network, E) mesosome-leucosome contact showing evident grain size increase and chlorite replacement after biotite; Pink granite leucosome F) plagioclase sub-rounded inclusion in a subidiomorphic microcline megacryst, with corroded borders forming graphic intergrowths (plagioclase and quartz) in the contact with quartz, G) microstructure of the paleosome amphibolite; Dark gray gneiss showing: H) typical microstrucure, note plagioclase diverse forms, I) cordierite spinel straight boundaries, J) hornblende grain with corroded shapes and bordered by quartz beads, plagioclase grains polygonal arrangemet, K) xenomorphic quartz-plagioclase; L) microstructure of the metagabbro

Table 1: Whole rock geochemistry of mafic rocks.

	Xingu Orthogneiss			**Amphibolite (mesosome)**					
Sample	5B	7B	22A	3-C2	3-C3	3-C5	3-C6	3-C7	3-C8
Major elements (wt%)									
SiO_2	48.50	48.5	49.14	49.87	49.23	49.59	47.34	51.01	46.47
TiO_2	0.75	0.887	1.157	0.25	0.82	0.52	0.70	0.28	0.66
Al_2O_3	14.80	14.71	13.8	15.19	15.30	16.68	14.07	14.74	16.05
Fe_2O_3	12.10	12.32	12.06	8.66	12.33	10.70	15.06	8.95	14.42
MnO	0.20	0.157	0.21	0.16	0.20	0.16	0.23	0.17	0.14
MgO	8.38	8.18	7.37	8.89	6.48	6.44	7.89	8.78	7.56
CaO	10.39	10.97	11.2	10.48	9.73	9.25	9.46	10.60	8.85
Na_2O	2.90	2.58	3.08	2.27	2.34	3.00	1.81	2.28	2.31
K_2O	0.79	0.68	0.75	1.63	1.10	1.27	1.19	1.19	1.73
P_2O_5	0.07	0.08	0.114	0.02	0.08	0.02	0.06	0.02	0.06
LOI	0.64	0.5	0.77	2.14	2.13	1.67	1.81	1.76	1.41
Total	99.50	100.1	99.70	99.60	99.70	99.30	99.60	99.80	99.70
Trace elements (ppm)									
Cr	380.55	247.5	233.92	475.32	226.05	131.36	260.16	225.11	260.27
Co	43.15	41.9	42.51	32.74	40.61	33.01	41.26	34.90	39.97
Sr	150.60	111.9	174.59	197.13	200.12	175.17	176.70	199.76	166.69
Y	19.56	24.6	26.04	7.97	22.28	12.37	24.57	9.89	17.05
Zr	37.21	52.7	37.63	8.80	50.14	14.58	40.67	10.87	40.18
V	257.82	270.32	322.24	137.14	238.23	251.94	249.32	167.06	196.69
Nb	5.02	2.6	2.65	1.71	3.22	4.12	3.43	1.83	2.38
Ta	0.28	0.18	0.20	0.28	0.45	0.73	0.33	0.51	0.26
La	6.18	3.8	5.69	2.71	5.08	3.68	9.31	2.79	5.97
Ce	15.59	9.7	11.41	5.55	11.90	9.21	25.56	5.66	13.52
Pr	2.03	1.5	1.85	0.72	1.59	1.06	3.27	0.69	1.58
Nd	8.79	7.3	8.68	2.85	7.55	4.49	14.37	3.01	6.95
Sm	2.43	2.5	2.93	0.89	2.36	1.26	3.68	0.92	1.88
Eu	0.79	0.9	0.97	0.42	0.88	0.41	1.10	0.46	0.76
Gd	2.55	3.0	3.34	0.93	2.69	1.43	3.66	1.11	2.15
Tb	0.47	0.6	0.66	0.19	0.50	0.27	0.64	0.22	0.40
Dy	3.25	4.4	4.69	1.36	3.69	1.97	4.33	1.53	2.87
Ho	0.68	1.0	1.04	0.30	0.78	0.40	0.89	0.34	0.60
Er	1.89	2.7	2.94	0.88	2.19	1.21	2.49	0.98	1.70
Tm	0.28	0.4	0.41	0.13	0.33	0.19	0.37	0.15	0.26
Yb	1.82	2.7	2.83	0.90	2.14	1.29	2.43	1.01	1.67
Lu	0.28	0.4	0.44	0.14	0.33	0.20	0.37	0.16	0.25
Hf	1.27	1.7	1.35	0.35	1.66	0.59	1.34	0.45	1.25
Pb	3.09	2.3	12.37	4.33	3.32	4.51	2.53	3.18	4.00
Th	0.13	0.4	0.14	0.59	1.10	0.52	1.08	0.72	1.64
U	0.10	0.7	0.23	0.71	1.13	0.65	0.40	1.66	0.67

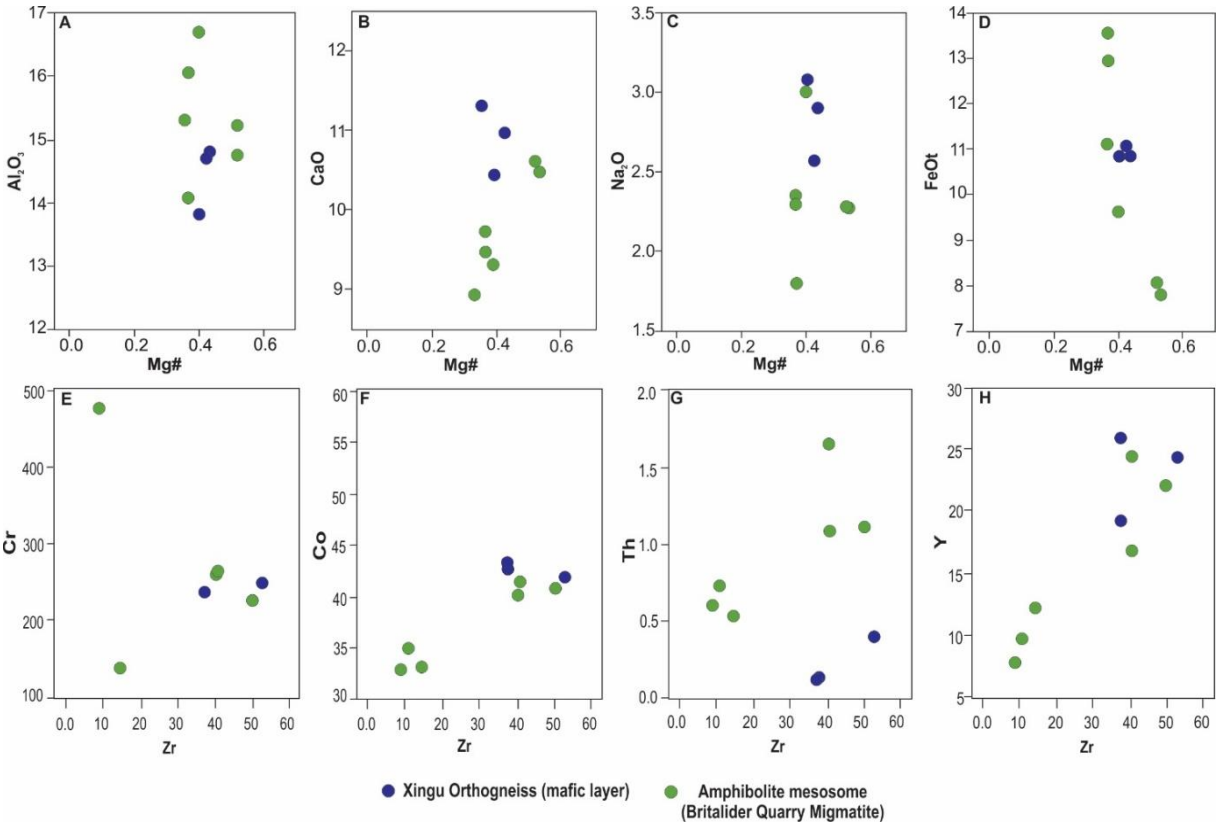

Fig. 8: Variation diagrams of: A to D) Major oxides against Mg# and E to H) Trace-elements against Zr. Major oxides in wt (%) and trace elements in ppm.

The variation diagrams of Zr, a less mobile element, against trace elements do not display an evident series correlation (Figs. 8E to H). These diagrams reveal instead two distinct groups concerning Zr content of amphibolite mesosome samples; the Zr-poor group (8.8 to 14.6 ppm) and the relatively Zr-rich group (40.2 to 50.1 ppm). The latter is also richer in TiO_2 (0.7 to 0.82 wt%) and its trace elements content range within Xingu orthogneiss samples, except for higher Th (1.1 to 1.6 ppm).

The binary variation diagram with Zr against K shows dispersed data for amphibolite mesosome samples, illustrating a very low correlation coefficient (r=0.48) between these elements (Fig. 9A). On the contrary, Ti and Zr are highly correlated (r=0.81) and display an almost linear array that encompasses both sample sets in the variation diagram (Fig. 9B). This mobility test reinforces LILe mobile behavior in comparison to HFSe in the studied scenario.

Considering the geochemical modifications promoted by metamorphism and hydrothermal alteration, this study applies immobile element geochemistry for mafic rocks classification, as proposed by Pearce (2014). In the Zr/Ti *vs*. Nb/Y diagram (Pearce 2014) all samples plot in the basalt field and exhibit affinity with those of the tholeiite series (Fig 10A).

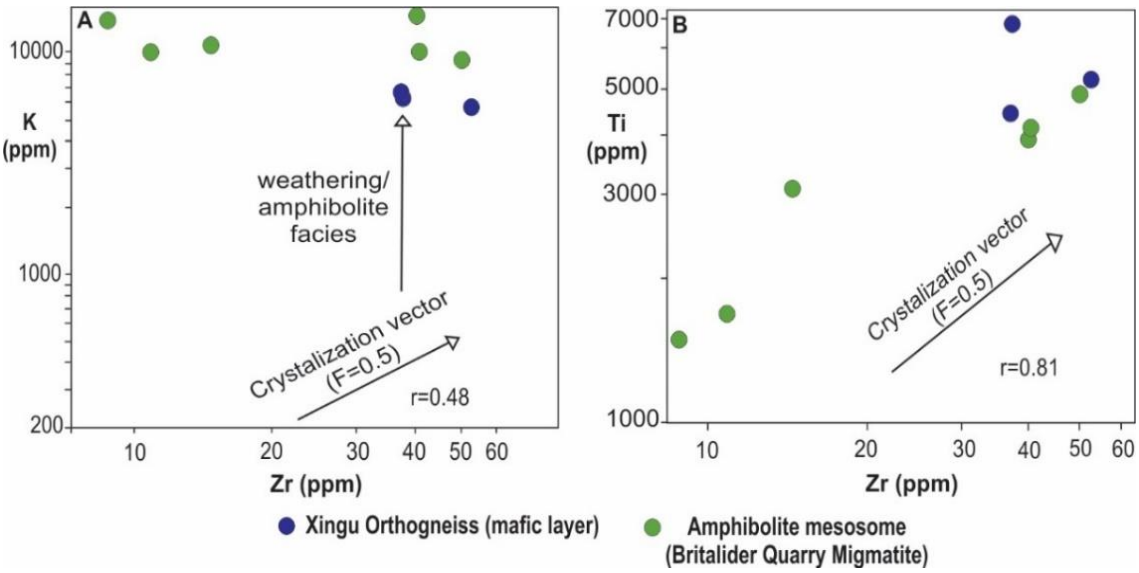

Fig. 9: Elements mobility test (Cann 1970): A) K vs. Zr diagram, B) Ti vs. Zr diagram.

Figure 10B shows the immobile elements MORB-normalized (Sun and McDonough 1989) spidergram as proposed by Pearce (2014) for pattern identification of ophiolite lavas in diverse modern settings. The Xingu orthogneiss samples envelope is narrow and coherent, presenting a discrete LREE enrichment in comparison to HREE with La/Yb_N ratio range from 1.74 to 4.41. This pattern resembles those of ophiolite lavas of contaminated mid-ocean ridge basalt (C-MORB) composition found in distal suprasubduction zone (SSZ) setting. The amphibolite mesosome envelope is wider and though displays a more LREE enriched and HREE depleted pattern, the La/Yb_N ratio range within the Xingu orthogneiss (2.9 to 4.68).

Proxies for tectonic discrimination distinguish the Xingu orthogneiss from the amphibolite mesosome. The former sample set plot close to MORB array (Fig. 10C). According to Pearce (2014), this diagonal data displacement may indicate lava modification due to continental crust assimilation, as suggested by C-MORB multi-element pattern resemblance (Fig. 10B). The amphibolite mesosome sample set present higher Th/Yb ratio and therefore plot along oceanic and continental arcs fields' intersection (Fig. 10C). In the V *vs*. Ti diagram, the Xingu orthogneiss plot in the transition from MORB (also slab distal back-arc basin and fore-arc basalts) to island-arc tholeiites fields (IAT & slab proximal, back-arc basin and fore-arc basalts). The amphibolite mesosome data dominantly spread in the IAT field (Fig. 10D).

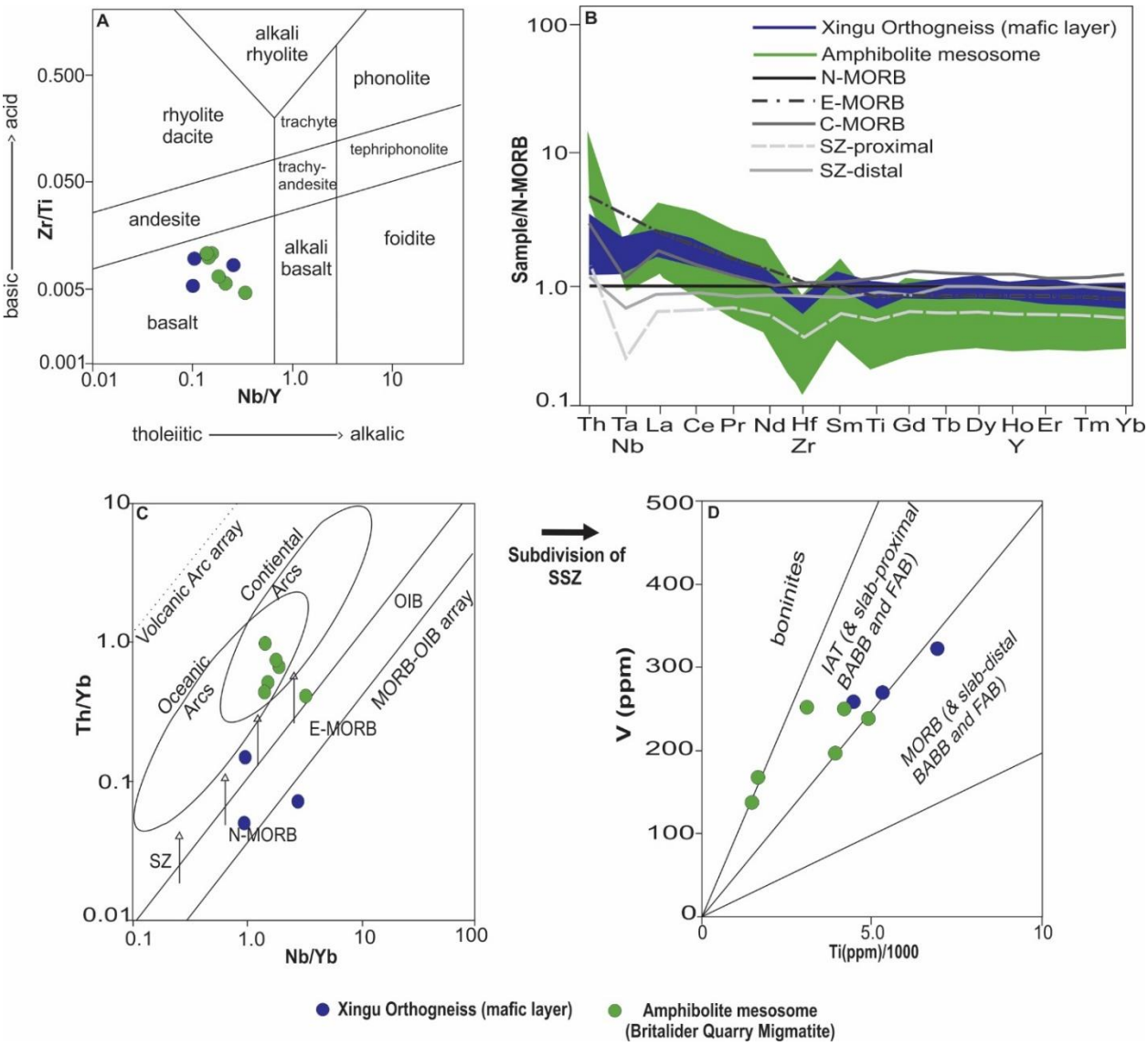

Fig. 10: Classification diagrams of Pearce (2014) for ophiolite sequences. A) Immobile element–based TAS proxy diagram; B) Multi-element MORB normalized spidergram (Sun & McDonough 1989) with data from Pearce (2014); C) The Th/Nb proxy used to distinguish suprasubduction zone (SSZ) from mid-ocean ridge ophiolites; D) The V/Ti subduction-melting proxy to distinguish MORB, island arc tholeiite (IAT), Back arc basin basalt (BABB), Fore arc basalt (FAB) and boninite magma types.

Major and trace elements of rocks from Britamil Quarry

The seven samples of the Tonalite gneiss mesosome are characterized by SiO_2 content ranging from 71 to 73 wt% (Table 2). Harker bivariate diagrams (Fig. 11) show that TiO_2, Al_2O_3 and FeOt have a negative correlation with SiO_2. Correlations between SiO_2, CaO and Na_2O are less evident, although they tend to a negative pattern, whereas K_2O exhibits a cloudy to slightly positive correlation with SiO_2.

Table 2: Whole-rock geochemistry of Britamil Quarry samples.

	Dark Gray Gneiss	**Tonalite Gneiss Mesosome**							**Pink Granite**		
Sample	1H4	1G1	1G2	1G3	1G4	1G5	1G6	1G7	1J1	1J2	1J3
Major elements (wt%)											
SiO_2	60.49	71.45	72.21	71.42	72.03	70.64	71.71	72.46	75.9	73.85	72.79
TiO_2	0.839	0.181	0.112	0.183	0.185	0.219	0.156	0.165	0.062	0.073	0.039
Al_2O_3	17.79	15.5	15.09	15.44	15.35	15.67	15.32	15.09	12.69	14.27	14.54
Fe_2O_3	5.36	1.58	1.03	1.49	1.47	1.67	1.28	1.24	0.32	0.76	0.55
MnO	0.073	0.02	0.016	0.027	0.021	0.021	0.02	0.017	0.007	0.01	0.005
MgO	1.99	0.48	0.28	0.47	0.45	0.52	0.46	0.39	0.18	0.11	0.05
CaO	4.52	2.21	1.71	1.86	2.07	2.38	1.66	1.87	0.6	1.03	0.55
Na_2O	5.27	5.13	4.71	5.38	5.2	5.14	5.26	4.93	2.62	3.84	3.19
K_2O	1.55	2.5	3.66	2.46	2.55	2.38	2.96	2.9	6.38	5.23	7.49
P_2O_5	0.211	0.07	0.05	0.07	0.07	0.08	0.06	0.07	0.02	0.09	0.02
LOI	1.23	0.67	0.55	0.67	0.69	0.73	0.72	0.57	0.5	0.41	0.39
Total	99.3	99.8	99.4	99.5	100.1	99.5	99.6	99.7	99.3	99.7	99.6
Trace elements (ppm)											
Zn	74.97	28.50	22.06	28.62	27.02	26.04	24.73	23.19	18.11	13.61	10.43
Rb	58.82	56.43	82.56	52.29	37.42	22.88	73.34	31.02	122.03	95.40	144.02
Sr	546.16	413.87	371.53	255.43	224.79	185.95	353.61	226.67	197.98	223.33	129.30
Y	6.32	2.52	2.13	2.36	2.15	2.26	1.86	1.62	0.93	3.28	0.70
Zr	162.07	115.36	82.14	98.67	93.73	106.69	93.90	97.27	33.77	51.78	74.57
Nb	5.99	2.71	1.64	2.28	2.34	4.08	1.59	1.80	2.48	1.08	0.54
Ta	0.36	0.06	0.06	0.14	0.08	0.07	0.07	0.14	0.25	0.09	0.08
Ba	851.00	744.00	961.43	697.55	691.39	855.31	746.54	1031.94	1953.91	1468.98	1434.89
La	29.84	14.75	11.25	10.73	10.13	9.21	13.23	9.65	10.41	12.81	4.05
Ce	55.70	25.05	19.09	24.73	15.42	11.57	22.44	14.92	12.67	20.81	2.87
Pr	6.58	2.57	2.06	1.86	1.92	1.56	2.43	1.89	1.73	2.66	0.58
Nd	24.18	8.36	6.75	6.26	6.40	5.18	7.91	6.45	5.21	9.00	1.82
Sm	4.50	1.38	1.14	1.10	1.10	0.91	1.38	1.05	0.75	1.71	0.33
Eu	1.51	0.68	0.55	0.45	0.46	0.62	0.52	0.52	0.68	0.64	0.55
Gd	3.41	1.14	0.89	0.93	0.86	0.79	0.98	0.78	0.54	1.32	0.26
Tb	0.40	0.12	0.10	0.09	0.09	0.09	0.10	0.08	0.05	0.16	0.03
Dy	1.69	0.56	0.43	0.43	0.45	0.48	0.38	0.31	0.20	0.77	0.15
Ho	0.25	0.09	0.08	0.07	0.07	0.08	0.07	0.06	0.04	0.13	0.03
Er	0.58	0.25	0.20	0.21	0.20	0.20	0.18	0.17	0.11	0.34	0.09
Tm	0.06	0.03	0.03	0.03	0.02	0.02	0.02	0.02	0.01	0.04	0.01
Yb	0.33	0.17	0.17	0.16	0.15	0.14	0.14	0.14	0.09	0.26	0.11
Lu	0.05	0.03	0.03	0.03	0.03	0.03	0.03	0.02	0.02	0.04	0.02
Hf	4.44	3.25	2.59	2.82	2.72	3.03	2.79	2.94	1.16	1.74	4.37
Pb	9.17	11.33	14.71	8.57	11.40	9.84	11.25	10.06	14.65	9.53	14.44
Th	6.07	1.65	2.10	4.04	2.33	0.55	3.33	2.13	3.75	3.74	2.28
U	0.84	0.37	0.78	1.06	0.50	0.40	0.83	0.64	1.27	0.45	3.18

In the Ab-An-Or ternary diagram (O´Connor 1965), normative compositions of the Tonalite gneiss mesosome plot in the trondhjemite field (Fig. 12A). In the K-Na-Ca diagram, samples concentrate in the Archean TTG´s field (Fig.12B). According to Frost et al. (2001) and Shand (1943) classification schemes, this unit corresponds to magnesian (Fig. 12C), slightly peraluminous granitoids (Fig 12D), mainly of calk-alkalic composition (Fig 12E).

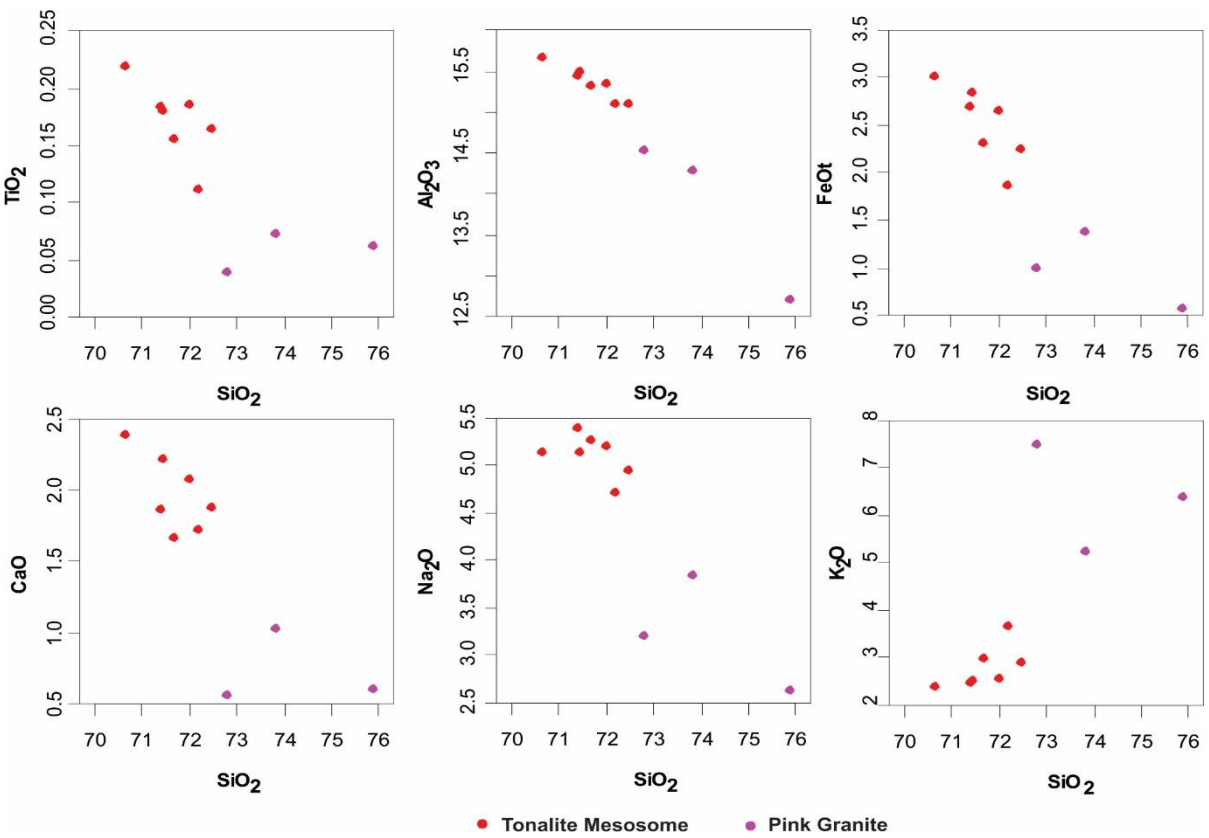

Fig. 11: Harkers variation diagrams of major elements vs SiO_2. Concentrations are in Wt(%).

The silica content of the Pink granite range from 72 to 75 wt%. Harker variation diagrams show no correlations between major elements and silica (Fig. 11). Normative compositions spread in the granite field of Ab-An-Or ternary plot (Fig. 12A) (O´Connor 1965). In the K-Na-Ca diagram, samples are disposed along calk-alkaline trend (Fig. 12B). In the Frost et al. (2001) diagram, samples inconclusively scatter in both ferroan and magnesian fields (Fig. 12C), though are classified as alkali-calcic to alkali composition granitoids of peraluminous character (Figs. 12D,E) (Shand 1943).

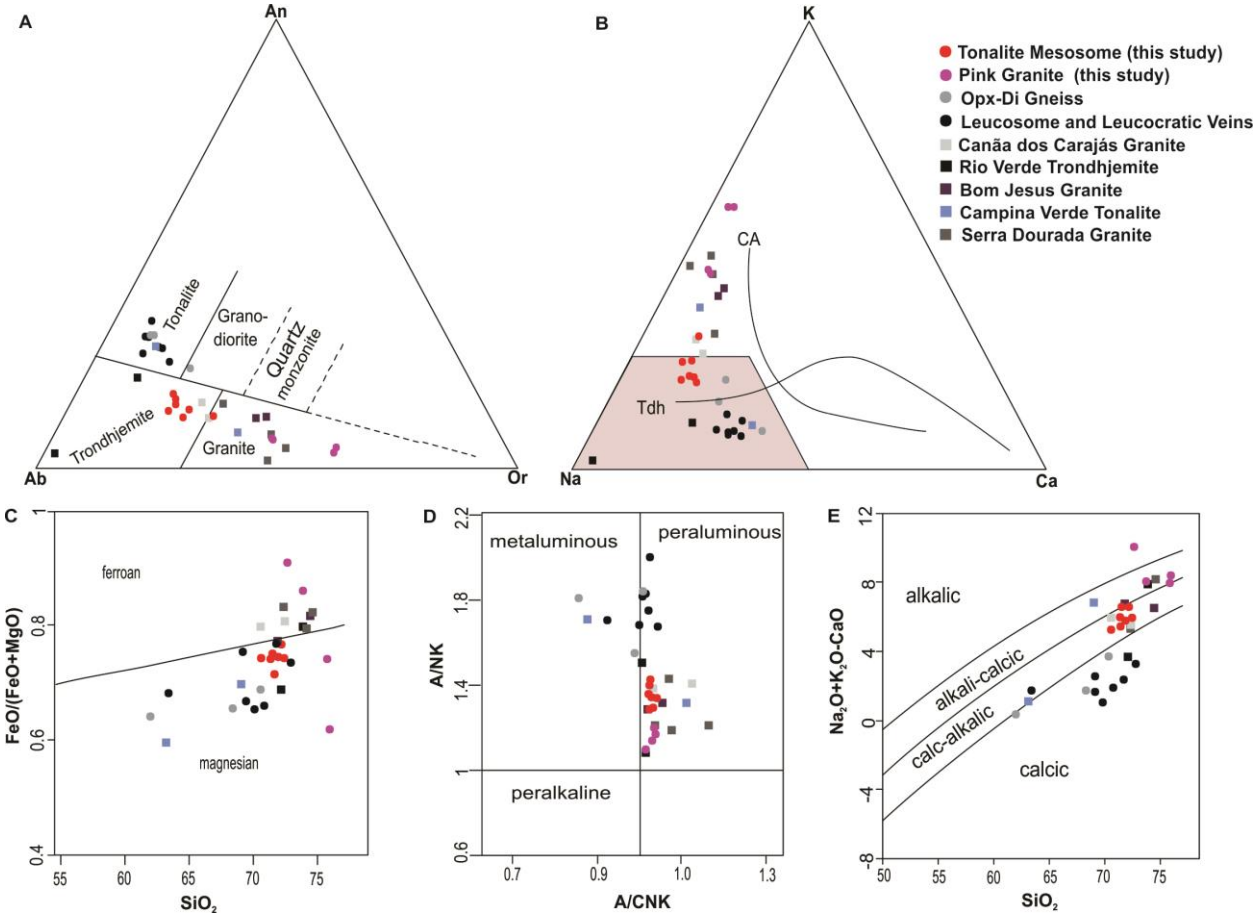

Fig. 12: Granitoids Classification Diagrams: A) Normative feldspar triangle (O´Connor 1965) with fields from Barker 1979, B) K-Na-Ca ternary diagram with trends from Barker and Arth (1976) and Archean TTG field from Martin (1994), C) SiO_2 vs. Fe number diagram (ferroan and magnesian granites fields of Frost et al. (2001), D)Alumina saturation index (Shand 1943), E) MALI-index vs. SiO_2 diagram (Frost et al. 2001).

Primitive mantle-normalized (Mcdounogh and Sun 1995) incompatible elements patterns are roughly similar for the Tonalite gneiss mesosome (Fig. 13A) and the Pink granite (Fig. 13B) samples. Despite a few differences in concentrations, both sample sets show LILe enrichment in comparison to HFSe. Nb-Ta negative anomaly and a marked Pb positive anomaly are also present in both units, though are more expressive in the Pink granite samples. One sample of the Pink granite present a Zr positive anomaly.

The Tonalite gneiss mesosome samples display a homogeneous pattern in the chondrite-normalized (Nakamura 1974) Rare earth elements (REE) diagram (Fig. 13C), with total REE ranging from 36 to 55.2 ppm. LREE enrichment relative to HREE, high La/Yb_N (44 to 62) (Fig. 13E) and Sr/Y (82 to 189) ratios (Fig. 13F) and europium slightly positive anomaly, Eu/Eu* 1.31 to 2.19 (Fig. 13G). The Pink granite REE pattern is sub-parallel to the Tonalite gneiss mesosome pattern (Fig 13C), though the former defines a broader range, with total REE ranging from 10.9 to 50.7 ppm and La/Yb_N from 25 to 78 (Fig. 13E). The Pink granite has more pronounced HREE concave shape (Fig 13C) and larger europium positive

anomaly (Eu/Eu* 1.3 to 7.9) (Fig. 13G) compared to the Tonalite gneiss mesosome. The Dark gray gneiss REE pattern presents a similar slope to the Tonalite gneiss mesosome (La/Yb_N 62), though it lacks in Eu anomaly (Eu/Eu* 1.14), and also differs its higher total REE content (129 ppm) (Fig. 13C).

In the tectonic discriminant diagram of Pearce et al (1984), samples of the tonalite gneiss mesosome plot in volcanic arc granites (VAG) field, whereas the Pink granite samples plot in a transition from VAG to syn-colisional granites field (syn-COLg) (Fig 13H).

ZIRCON DATING U-PB (LA-ICP-MS)

A set of four samples were selected for zircon U-Pb LA ICP-MS geochronology. The analyzed samples correspond to: i) Tonalite Diatexite (3A1) of the Britalider Quarry; and ii) Tonalite gneiss Mesosome (1G1), iii) Pink granite vein (1J1) and iv) Dark gray gneiss (1H4) of the Britamil Quarry. Analytical data and uncertainties are shown in table 3.

Tonalite diatexite

Zircon grains of sample 3A1 are light-pink translucent to white, subidiomorphic, have oval or prismatic shapes with sub-rounded terminations. Zircon fragments are also observed. Crystal length ranges from 48 to 162 μm, with elongation ratio from 1 to 2. Grains may show no internal texture, concentric oscillatory or vague sector zoning (Figs. 14A to C). Th/U ratio ranges from 1.81 to 6.16. Seven spot analyses yielded a concordia age of 2862.5 ±6.2711 Ma (MSWD 0.24; Fig. 15A).

Tonalite gneiss Mesosome

Zircon grains of sample 1G1 are pink, idiomorphic to subidiomorphic, either oval-shaped or prismatic with rounded to flat terminations. Crystal lengths range from 60 to 262 μm with lenght/width ratio from 1 to 3. Th/U ratio ranges from 0.4 to 1.02. Most grains do not present internal texture (Figs. 14D to F), though discrete resorption shapes and oscillatory zoning are identified in some grains. Fourteen spot analyses provided a concordant age of 2855.6 ± 2.75 Ma (MSWD=1.45; Fig. 15B).

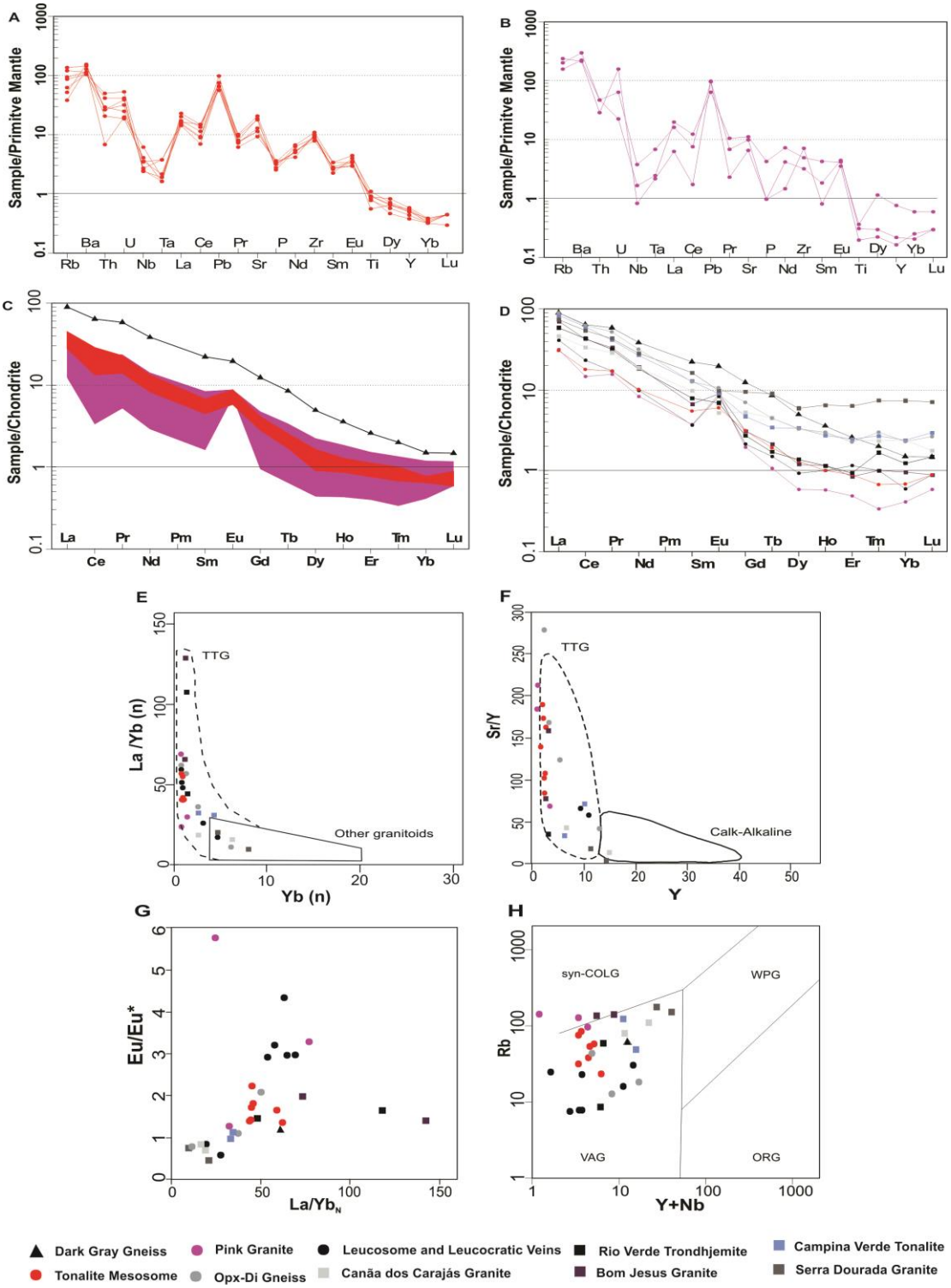

Fig. 13: Trace element geochemistry: Primitive mantle-normalized (Mcdounogh and Sun 1995) multi-element pattern for: A) Tonalite gneiss mesosome samples and B) Pink granite samples. Chondrite-normalized (Nakamura 1974) REE pattern for: C) this study samples; D) this study, Delinardo da Silva et al (2015) and Feio et al (2012, 2013) representative samples. Bivariate diagrams with fields from Martin et al 1999,:E) La/Yb(n) vs Yb(n), F) Sr/Y vs Y. G) Eu/Eu* vs. La/Yb. H) Tectonic discriminant with fields from Pearce et al (1984).

Table 3: Geochronological data of Britalider and Britamil Quarries samples

	Isotopic Ratios								ages (Ma)				
Zircon Grain	Comm. 206(%)	U (ppm)	Th (ppm)	Th/U	207Pb/ 235U	1σ	206Pb/ 238U	1σ	207Pb/ 206Pb	2σ	206Pb/ 238U	2σ	% conc
Sample 3A1													
6	0.09	75.6	354.5	4.689	15.68	2.0	0.556	2.2	2866	18	2840	52	99.1
10	0.08	79.2	346.5	4.375	15.78	1.7	0.561	1.7	2851	15	2870	41	100.7
12	0.06	116	715	6.164	15.73	1.8	0.558	2.2	2871	18	2847	50	99.2
14	0.04	136.2	246.8	1.812	15.64	1.8	0.558	2.0	2847	16	2852	44	100.2
22	0.11	58.1	240.3	4.136	15.82	1.6	0.560	1.8	2860	16	2856	42	99.9
34	0.16	39.4	180.8	4.589	15.8	1.8	0.557	2.0	2881	17	2840	46	98.6
Sample 1G1													
1	0.01	302	308	1.020	15.52	1.5	0.558	1.52	2842	11	2860	36	100.6
4	0.01	284.2	231.8	0.816	15.86	1.5	0.557	1.60	2878	10	2858	36	99.3
9	0.02	210.6	198.4	0.942	15.39	1.0	0.555	1.24	2857.2	8.4	2842	28	99.5
10	0.01	335.7	337.1	1.004	15.71	1.4	0.560	1.64	2853.7	9.6	2871	37	100.6
44	0.02	221.2	201.9	0.913	15.67	1.1	0.559	1.31	2856.3	7.8	2858	30	100.1
45	0.02	251.7	227.6	0.904	15.7	1.1	0.557	1.18	2853.7	9	2854	27	100.0
48	0.02	279.5	274.2	0.981	15.69	1.0	0.557	1.06	2859.1	7.5	2850	24	99.7
50	0.02	197.8	197.7	0.999	15.73	1.1	0.561	1.25	2850.9	8.7	2865	29	100.5
51	0.02	232.8	194.5	0.835	15.65	1.1	0.554	1.17	2856.6	8.9	2841	27	99.5
55	0.03	153.2	132.7	0.866	15.71	1.1	0.557	1.35	2863.3	9.9	2850	31	99.5
57	0.02	287.8	257	0.893	15.61	1.7	0.561	1.76	2846	11	2866	41	100.7
59	0.02	229.1	215.9	0.942	15.92	1.4	0.564	1.65	2857	11	2888	37	101.1
61	0.01	336	278.4	0.829	15.65	0.9	0.559	1.00	2851.4	8.3	2864	23	100.4
64	0.01	373	149.5	0.401	15.6	1.2	0.558	1.20	2845.3	8.8	2865	27	100.7
Sample 1J1													
15	0.04	139.4	89.6	0.643	15.96	1.4	0.568	1.52	2833	14	2898	36	102.3
16	0.03	186.4	119.3	0.640	16.17	1.4	0.567	1.62	2885	12	2897	38	100.4
22	0.01	512	137.1	0.268	16.02	1.3	0.566	1.48	2861	10	2886	35	100.9
23	0.03	192.7	121.7	0.632	15.94	1.3	0.560	1.45	2862	11	2864	33	100.1
25	0.02	328	186.9	0.570	16.1	1.2	0.566	1.40	2868	10	2887	33	100.7
26	0.02	387	162.5	0.420	16.02	1.6	0.565	1.77	2864	12	2878	41	100.5
30	0.03	218.6	90	0.412	16.01	1.3	0.561	1.51	2867	11	2869	35	100.1
34	0.03	179.2	124.6	0.695	15.96	1.4	0.560	1.34	2854	11	2862	31	100.3
Sample 1H4													
4	0.02	191.6	139	0.725	16.13	1.4	0.562	1.48	2883	11	2877	35	99.8
11	0.03	188.8	136	0.720	16.06	1.2	0.565	1.26	2857	10	2889	29	101.1
21	0.02	344.6	220.8	0.641	16.21	1.2	0.567	1.46	2871	9.7	2886	34	100.5
26	0.02	368	226.5	0.615	16.02	1.2	0.564	1.35	2857	11	2882	31	100.9
28	0.02	280.5	231.1	0.824	16.12	1.4	0.563	1.56	2873	12	2872	36	100.0
43	0.02	339	212.6	0.627	16.3	1.3	0.567	1.46	2885	12	2891	34	100.2

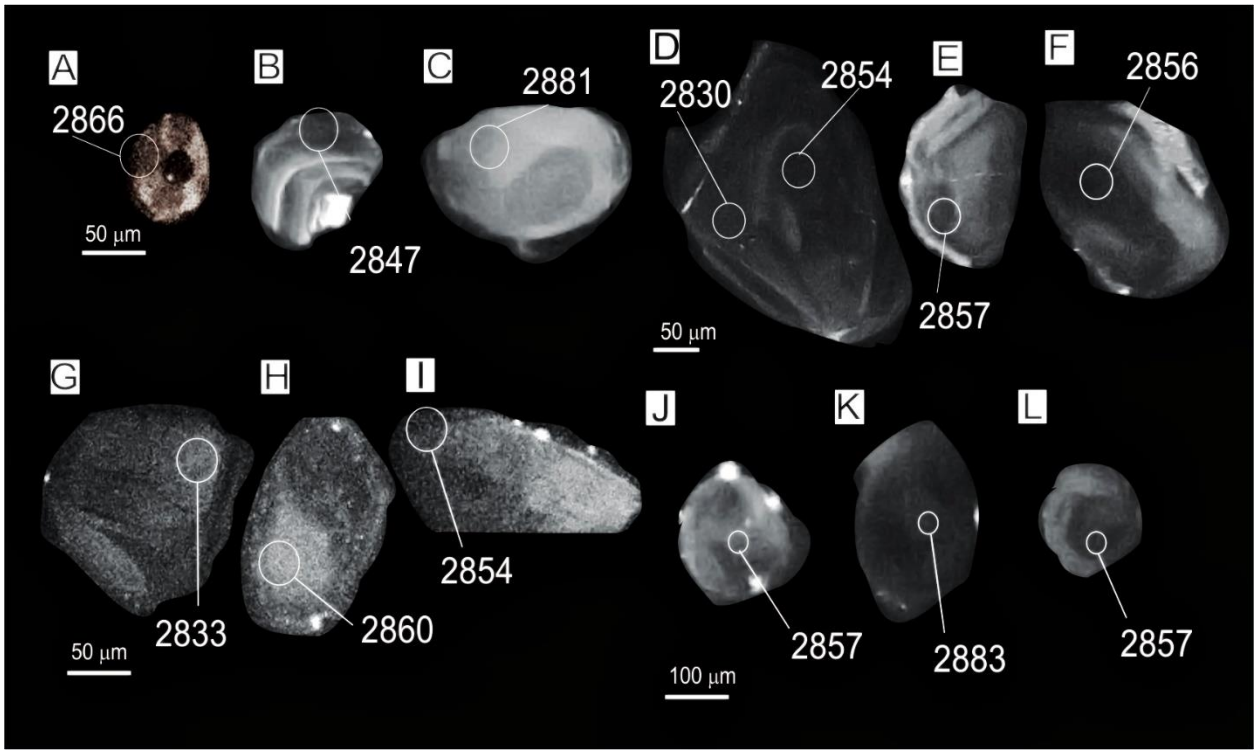

Fig. 14: CL images of zircons of A, B, C) Tonalite Diatexite (Britalider quarry); D, E, F) Tonalite gneiss mesosome (Britamil quarry), G, H, I) Pink granite (Britamil quarry); J, K, L) Dark gray gneiss (Britamil quarry). $^{207}Pb/^{206}Pb$ ages are indicated at the analyzed spot.

Pink granite

Zircon grains of sample 1J1 are homogenous translucent pink or present white core overgrown by light pink tip. Crystals are subidiomorphic to xenomorphic with highly resorbed or ovoid shapes, though exists prismatic variations with pyramidal to sub-rounded terminations. Most grains do not display internal texture, but some present core and rim structure, with brighter rim (Figs. 14G to I). Crystal length ranges from 70 to 162 µm, with aspect ratio from 1 to 3. Th/U ratios ranges from 0.27 to 0.7. Eight spot analyses yielded a concordant age of 2877.3 ±4.228 Ma (MSWD=0.6; Fig. 15C). A discordia obtained by 30 spot analyses projects an upper intercept age of 2864.4 ±6.196 Ma (Fig. 15D).

Dark gray gneiss

Zircon grains of sample 1H4 are dominantly murky pink colored, subidiomorphic and ovoid. Crystals may lack in internal textures or present weak oscillatory zoning with xenocrystic darker cores. (Figs. 14J, K, L). Crystal length vary from 122 to 334 µm, with elongation from 1 to 2, except for one highly prismatic grain, in which elongation is around 5. Th/U ratios range from 0.45 to 0.86. Six spot analyses provided a concordia age of 2884.7 ± 4.6529 Ma (MSWD=0.74, Fig. 15E).

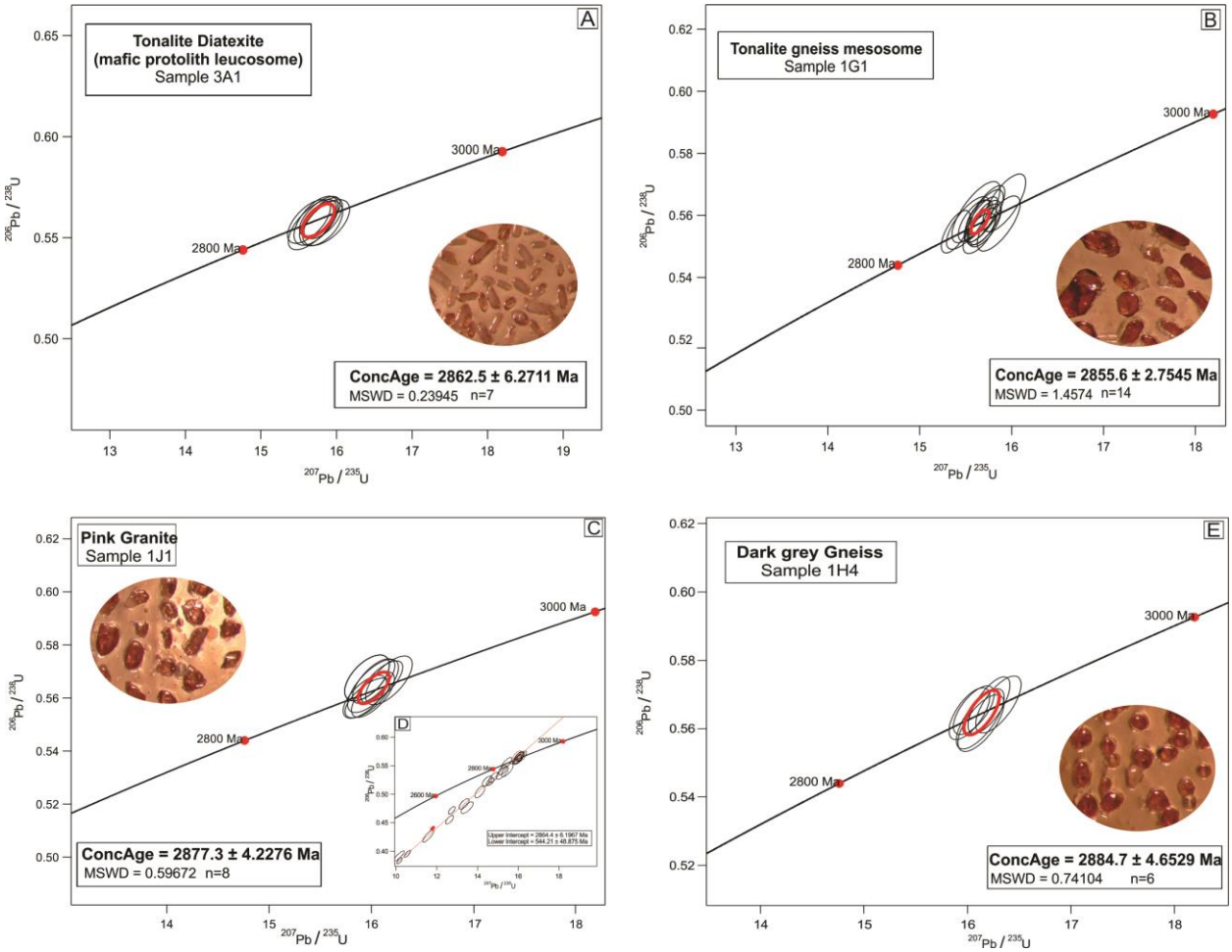

Fig. 15: $^{206}Pb/^{238}U$ vs. $^{207}Pb/^{235}U$ diagrams of zircons of the rocks analyzed by U–Pb LAICP-MS and zircon grains aspect under magnifier for: A) Tonalite Diatexite of the Britalider Quarry and Britamil Quarry: B) Tonalite gneiss mesosome, Pink granite leucosome, C) concordia age and D) alternative discordia age, E) Dark gray gneiss.

DISCUSSIONS

We aim to discuss the petrogenesis of the Xingu Migmatites and implications for the Carajás basement evolution during the Mesoarchean based on field, microstructural, geochemical and geochronological data. Thus, the points to address are: i) The protolith nature; ii) metamorphism, melting products and melting mechanisms; and iv) timing and setting of anatexis.

The Protolith

Archean high-grade terranes largely include granitoid rocks and variable proportions of amphibolite arranged as gray to banded gneisses complexes (Moyen 2011). These gneiss units commonly show evidence of partial melting, being also referred as gneiss-migmatite complexes (White et al 2017). According to Sawyer (2010), in a migmatite, the neosome-host rocks are the closest estimate to the protolith. The neosome host-rocks may also be referred as mesosome or paleosome, as they represent incipiently melted to unmelted rocks, respectively, chemically modified during partial melting (Vernon 2008). The mesosome at the Britalider quarry corresponds to amphibolite boudins and schollen, which host and interleave a large volume of tonalitic leucosome (Fig. 3). In the Britamil quarry, amphibolite paleosome and tonalite gneiss mesosome coexist and host granodioritic to granitic leucosomes (Fig. 6). The roughly bimodal character of the migmatites presented in this study in both quarries suggest a composite banded orthogneiss protolith as the heterogeneous source for the Xingu migmatites.

Banded orthogneisses represent exhumed slices of the thickened continental crust and comprise a wide range of rock material from mafic to felsic components (White et al 2017). In the northeastern Carajás area, the Xingu banded Orthogneiss corresponds to the highest metamorphic-grade rock with minimum leucosome content among the studied litotypes (Fig. 2). The mafic layers are clinopyroxene-bearing amphibolite in paragenesis with calcium-rich plagioclase, suggesting though at least upper amphibolite facies metamorphism (Binns 1965). This pressure-temperature field is consistent with the conditions required for crustal melting as reported in numerous studies (e.g.: White 2005, Weinberg 2016, Brown 2012, Kunz et al 2014, Weinberg & Hasalová 2015). Furthermore, the minerals in the mafic layers preserve disequilibrium textures such as lobate shapes and cuspate grain junctions (Fig 2B, D), which are structures typically associated with the partial melting beginning (Sawyer 1999, 2001, Holness and Sawyer 2008, Vernon 2008, Brown 2012, Weinberg & Hasalová 2015). We

inferred that Xingu banded orthogneiss might correspond to rocks formed under conditions developed near a hypothetical melt-in isograd.

Field relationships and detailed petrography strongly suggest that the Xingu banded Orthogneiss most likely represent a parental gneiss of the Xingu migmatites at the Britalider Quarry. Considering the tectono-thermal events superimposed at the Britalider Quarry, represented by transposed and crosscutted foliations (Fig. 4), is difficult to assert a petrogenetic link between amphibolite mesosome and the mafic layers of Xingu banded orthogneiss even using immobile element geochemistry. Pearce (2014) stated that even immobile elements as U, Th Zr and Nb can experiment mobilization under the influence of shear zones. However, we may compare geochemical igneous fingerprints. The tectonic discriminant proxies (Figs. 10C, D) indicate that the mafic layers of the Xingu banded Orthogneiss and the Britalider quarry amphibolite mesosome may share a pre partial-melting metamorphic history under the influence of a subduction zone associated with an arc setting. This immobile-element concentration differences could be interpreted as a result of the subduction zone closeness, being the Xingu orthogneiss less affected (slab-distal) than the Amphibolite mesosome (slab-proximal).

The Xingu migmatites at Britamil quarry preserve the tonalite gneiss mesosome, (Fig. 6) suggesting that the metatexite closest protolith was a composite banded gray gneiss. As stated by Moyen (2011), the archean lower crust represents composite rock assemblage dominated by granitoids regarded as TTG series. According to Rudnick (1992), severe HREE depletion in felsic archean granulites of tonalitic to granitic compositions are common and documents the role of garnet in their petrogenesis. These trace-elements characteristics in addition to high La/Yb and low Y are typical of archean TTG magmatic series. In the Canaã dos Carajás area (southern Carajás Domain), samples of the orthopyroxene-diopside Gneiss, leucosome and leucocratic veins present geochemical affinity with TTG series (Fig. 13D) (Delinardo da Silva 2014), differently from the most mesoarchean calk-alkaline granitoids of south Carajás Domain (Campina Verde, Serra Dourada, and Bom Jesus), with exception of the Rio Verde trondjhemite (Feio et al 2013). The orthopyroxene-diopside Gneiss and leucosomes of Canaã dos Carajás share trace-element composition similarities with the Tonalite gneiss mesosome, though significantly older (3.0 and 2.96 Ga respectively; Delinardo da Silva 2014). The rare earth elements (REE) pattern show light REE (LREE) enrichment and heavy REE (HREE) depletion, with Eu positive anomaly (Fig. 13C). This same REE behaviour resemblance is verified for the Rio Verde trondhjemite and Bom Jesus

Granite. The HREE depletion and Eu positive anomaly are more conspicuous in this study samples (Fig. 13D).

Considering the high mobility of major elements during partial melting and fractionation during melt crystallization, trace element geochemistry is more reliable to determine magmatic series for the Tonalite gneiss mesosome igneous protolith. The La/Yb(n) vs Yb(n) and Sr/Y vs Y diagrams (Figs. 13E, F) indicate a TTG series affinity for the Tonalite gneiss mesosome protolith. The Eu positive anomalies may be source inherited or either related to partial melting event and consequent plagioclase accumulation. Although the trace element pattern for the Pink granite veins and lenses roughly resembles tonalite gneiss mesosome (Figs. 13A to D) and most samples plot close to TTG series field in bivariate diagrams (Figs. 13E, F), its composition significantly varies. As expected for late stage pegmatite-like leucosome, Pink granite data exhibits substantial scattering.

Metamorphism, melting products and melting mechanisms

The Britalider migmatites

The stromatic migmatite display leucosome parallel to mesosome layers, a structure likely inherited from the banded gneiss protolith (Fig. 6A). Schollen, schlieren and homogenous diatexites result from higher melting rates and larger accumulation of the former melt-phase. The schollen diatexite shows typical boudinage of the mesosome with leucosome accumulation in interboudin sites. Weinberg (2015) and Vernon (2008) pointed that the asymmetrical disposal of boudins and its disruption by leucosome veins suggest a shearing component synchronous to partial melting. Deformation allows melting migration and consequently accumulation to form larger bodies (Sawyer 1994, Brown & Solar 1998b Hasalová et al 2008a, 2008b). However, the voluminous leucosome fraction found at the Britalider quarry, requires an open system in which fluid entrance plays a key role, as expected for melting at upper amphibolite facies conditions (Brown 2012).The presence of a hydrous perithetic phase, such as hornblende, also supports the addition of external aqueous fluids during partial melting (Weinberg 2015).

However, the partial melting of an amphibolite protolith to produce the leucosome content present in this migmatite is unlikely even with water addition. Considering the Xingu banded orthogneiss as an heterogeneous protolith, we interpret that layers of tonalite composition melted at first via reaction I (Watkins et al 2007), followed by the partial melting of the amphibolite (mesosome) that also produced a tonalite leucosome. The presence of

abundant zircon in leucosome from diatexite facies and its absence in the amphibolite mesosome might corroborate with this hypothesis.

$$Hbl/Bt + Qtz + Pl/Kfs + H_2O = melt \ (I)$$

The in situ unsegregated neosome patches (tonalite leucosome + perithetic hornblende) within the amphibolite schollen and rafts indicate that melting occurred via reaction II (Lee & Cho 2013).

$$Amp + Pl + Qtz + H_2O = Hbl{+}melt \ (II)$$

The mineral assemblage dominated by hornblende and plagioclase with minor quartz in the Amphibolite mesosome at Britalider quarry is consistent with the paragenesis encountered in literature for subsolidus amphibolite facies metabasites, which may have or lack epidote, clinopyroxene, biotite or garnet (Palin et al 2016, Spear, 1993; Pattison, 2003). The absence of clinopyroxene in the mesosome and melanosome at the Britalider quarry might have two possible explanations: i) insufficient P and T conditions or ii) complete re equilibration via hydration forming amphibole (hornblende). The second option seems more reasonable as diopside is present in the protolith (Xingu banded orthogneiss) and symplectite-like hornblende-quartz intergrowth are observed in the mafic schlieren residue (Fig. 5C, F). This disequilibrium texture is typically associated with pyroxene breakdown via rapid decompression during exhumation from lower to mid crustal levels. There is no petrographic or microstructural evidence of perithetic clinopyroxene formation in neosome. However, as pointed by Vernon (2008) neosome crystallization in their source rocks releases water and initiate retrograde reactions by hydration of perithetic minerals and adjacent mesosome. The lack of clinopyroxene in these migmatites residue might be related to hydration during retrogression either via melt crystallization, via rapid decompression, or both, associated with the exhumation of these lower crust rocks.

Experimental and natural cases of amphibolite-facies migmatites studies report back reactions between neosome and residue during cooling (Timmermann et al 2002, Ashworth and McLellan 1985; Kriegsman and Hensen 1998). The authors describe features such as fine-grained aggregates of Bt–Pl–Qtz as a product of late stage cooling, similar to observed in diatexites of Britalider quarry (Fig. 5E).

Melt crystallization and water loss constitute a feedback relation promoting retrograde reactions (White & Powell 2010). We understand that, in this migmatite portion, melt migration was restricted and melting occurred very close to the wet solidus, as melt crystallization roughly occurred in source.

Crustal-scale shear zones represent the most likely pathway for water entrance and also constitute proper structures for tectonic scape during collisional orogens (Brown & Solar, 1997). The amphibolite mesosome folding (Fig. 4B), its boudins disruption by leucosomes and the foliation found in the schlieren diatexites (Fig. 4C) indicates melting was synchronous to shearing, most likely associated to a transpressional shear zone system. Identifying melt structures, such as microfilms and perithetic products in tonalitic layers is commonly difficult, especially when solid-state deformation and grain recovery processes modifies migmatites after melt crystallization (White et al 2017). Magmatic flow features were not observed, probably due to their obliteration, as suggested by the strongly marked schlieren sub vertical foliation. Microstructures of the foliated leucosome (e.g: plagioclase-quartz steeped sutured contacts) indicate that high-temperature deformation continued to act after melt crystallization (Fig. 5G). Core and mantle microstructure in quartz grains reveals the persistence of solid-state deformation and recovery in higher crustal levels (low temperature and low pressure; Fig. 5I).

The presence of hastingsite, scapolite, chlorite and sulphides, which occur as veins filling brittle to brittle-ductile fault planes, represent a hydrothermal overprint (e.g.: sodic and sodic-calcic alteration; and chloritization) in the metamorphic mineral assemblage and register the widespread hydrothermal events in the Carajás domain (Monteiro et al 2014 and references therein).

The Britamil quarry migmatites

Machado et al (1991) first described partial melt-derived rocks in the northeastern Carajás, at the Cimcop Quarry, currently known as Britamil Quarry. Barros et al. (2010) questioned the anatectic origin of these rocks mainly due to lack of clear field evidence. These authors argued a magmatic flow origin for the sub vertical foliation observed in tonalite rocks at the quarry. Previously, Machado et al (1991) recognized at least two migmatization episodes, the last represented by undeformed leucosome. As stated by Sawyer (1999), macroscopic textures are the simplest criteria to recognize partial melted rocks. The schlieren melanosome and blurring of the metamorphic banded-gneiss structure provides then main evidences for partial melting at the gneiss of the Britamil Quarry.

Indeed, diverse leucosome styles are identified: accumulate as diatexites, plagioclase-rich and microcline-rich veins or dykes; and late stage veinlets (Fig. 6), although in our understanding they express different stages of a single anatectic event, as further discussed. Undeformed leucosome, as described by Machado et al (1991), was not identified in this study. However, those authors´ contribution did not include detailed microstructural and petrographic analysis. In this study, even the least deformed pink granite leucosome veins show deformation under amphibolite facies conditions, as suggested by petrographic evidence such as polygonal matrix and flame perthite texture.

Although outcrop-scale evidence for partial melting can be debatable at the Britamil quarry (e.g., Barros et. al., 2010), microstructures, such as polymineralic aggregates in pockets or veins in the mesosome, leave fewer doubts about the presence of a former melt-phase. The Tonalite gneiss framework is dominantly granoblastic with preserved cuspate microfilms of quartz-feldspar at grain junction (Fig. 7A to C). Microcline veins fills interganular spaces and disrupt residual grains, forming a connected network (Fig. 7D). Microstructures indicate that the tonalite gneiss melted via reaction III (Watkins et al 2007), producing leucosome with a granodiorite composition.

$$Bt + Qtz + Pl/Kfs + H_2O = melt \quad (III)$$

In comparison to the Britalider Quarry, the Britamil migmatite reveals lower melting rates, as amphibolite paleosome remained unmelted, and melt accumulation as diatexites are less expressive. Therefore, the former melt content seems to increase towards north (Figs 1C, D). Considering the contribution of a tonalite composition protolith and similar upper amphibolite facies metamorphic conditions for both migmatites, it is suggested that the water availability during partial melting was higher at the Britalider quarry compoared to the Britamil quarry. Less water availability also implies less retrogression due to water diffusion to the host rock during crystallization (Weinberg 2015). The establishment of an intrusion relation between leucosome and the unreactant paleosome in the Britamil quarry (Fig 6B) might be explained by the insignificance of back reactions between paleosome and neosome, given the limited amount of water in the latter.

The study of Machado et al. (1991) mentions retrogressed granulites at the Britamil Quarry. Indeed, the Dark gray gneiss mineral assemblage (hercynite spinel and cordierite) is commonly associated with high-temperature granulite facies metamorphism (Waters 1991). The Dark gray gneiss displays evidence of a former melt phase presence, as

quartz-plagioclase microfilms at grain junction and quartz beads at grain boundaries (Fig. 7J, K). Despite that, the hydrate character of this unit (hornblende-bearing granulite) and trace element pattern with absence of Eu anomaly (Fig. 13C) suggests that the petrogenetic relationships between the dark gray gneiss and migmatites are not compatible with the granulite formation as the anhydrous residual product of melting. However, this unit records a significant increase in temperature, coincidentally or not, in a regional anatetic context. Field observations indicate that the dark gray gneiss is spatially associated with a metagabbro, though their relationship is unclear. It is known that a mafic intrusion can have local heat effects on contacting rocks and regional intrusion can affect the adjacent gneiss (Gao et al 2017). The timing of gabbro emplacement and subsequently metamorphism were not constrained in this study.

Timing and implications for the Carajás basement evolution during the Mesoarchean

Considering geological phenomena duration, the zircon U-Pb (LA-ICP -MS) ages obtained in this study define a relative restricted span of time. Dark gray gneiss of the Britamil Quarry is the oldest lithotype with a concordant age of 2884.7 ± 4.6529 Ma (MSWD=0.74; Fig. 15E). Tonalite diatexite of the Britalider Quarry yielded a concordant age of 2862.5 ±6.2711 Ma (MSWD 0.24; Fig. 15A). The tonalite gneiss mesosome and the Pink granite of the Britamil Quarry reached the concordant ages of 2855.6 ± 2.75 Ma (MSWD=1.45; Fig. 15B) and 2877.3 ±4.228 Ma (MSWD=0.6.; Fig. 15C), respectively. Alternatively, the upper intercept age of 2864.4 ±6.2 Ma was also calculated for the Pink granite (Fig. 15D)

Igneous zircons commonly present high Th/U, while metamorphic zircons commonly present Th/U lower than 0.1 (Rubatto, 2017). Nonetheless, high-grade metamorphic rocks, especially those that reached high temperature conditions, exceptionally present high Th/U ratios (Pidgeon, 1992, Rubatto 2002, Rubatto & Hermann, 2007, Rubatto, 2017)., The Th/U ratios alone are not a reliable criteria in order to determine zircon grain origin, though if combined with grain shape, textures and geological context they might provide some clues (Corfu et al. 2003 and references therein). The dark gray gneiss zircons are rounded shape with low aspect ratios, murky pink (Fig 15E) and have high Th/U ratio (0.45 to 0.86) that suggest metamorphic modifications. We then interpret that the ca. 2.88 Ga age records a metamorphic event at moderate pressure and high temperature in granulite

facies conditions, which is supported by the paragenetic association of hercynite spinel + cordierite.

Zircon presenting low luminescence, textureless domains, blurred primary oscillatory zoning and recrystallized domains indicate recrystallization of protolith zircon rather than new zircon growth during metamorphism and anatexis (Siebel et al 2012). These characteristics are found is zircon grains of the Tonalite Diatexite, the Tonalite gneiss mesosome and the Pink granite. The obtained ages of ca. 2.87 to 2.85 Ga are interpreted in this study as the last high metamorphic-grade event accompanied by anataxis, and postdates granulite facies metamorphism registered in the Dark gray gneiss.

The Th/U ratios of the Tonalite gneiss mesosome zircon are also high (04-1.02). The zircons are dominantly prismatic and pink translucent (Fig. 15B), and a magmatic origin associated with an anatectic melt crystallization is unlikely, as suggested by rock petrography and microstructure (gneissic foliation with granoblastic texture) and zircons resorbed shapes and recrystallized domains (Figs. 14D to F and 15B). Similar characteristics are also observed in the Pink granite zircons, differing only by the presence of white cores and more resorbed shapes. Since the Pink granite leucosome veins crosscut the Tonalite gneiss mesosome (2855.6 ± 2.75 Ma), the obtained age of 2877.3 ±4.228 may be interpret with caution. Factors controlling such ages disparities probably represent a confluence of analytical issues involving data reduction, grain zonation and isotopic inheritance. The Pink granite upper intercept age of 2864.4 ±6.196 Ma (discordia) (Fig. 15D) might be more suitable, as provides a closer temporal relation between it and the Tonalite gneiss mesosome.

The Tonalite Diatexite zircons register recrystallization at 2862.5 ±6.2711 Ma. The unusually high Th/U ratios (up to 6) from this sample can be attributed to deformation in the presence of a late-stage magmatic fluid, which drove elevated Th over U content (Timms et al 2006).

The ca. 2.87-2.85 Ga ages obtained in this study establish a meaningful time constraint. A magmatic event at ca. 2.86 Ga in the Carajás Domain has been well documented by several authors (Machado et al, 1991, Moreto et al 2011, Feio et al 2013, Melo et al 2016). According to Machado et al (1991), the partial melting of Xingu basement gneisses occurred at 2859 ± 2 Ma (U-Pb in zircon). Mesoarchean calk-alkaline granitoids of tonalite to trondjemite and granitic compositions units, variably deformed, yielded crystallization ages from 2.87 to 2.83 Ga (e.g: Canãa dos Carajás granite, Campina Verde Tonalite, Rio Verde Trondhjemite, Serra Dourada, Bom Jesus and Cruzadão Granites) (Moreto et al 2011; Feio et al 2013). At the Salobo area, Melo et al (2016) documented ore deposit host-rocks (Xingu orthogneiss) zircon populations with concordant age of 2857 ± 6.7 Ma (U-Pb Shrimp IIe).

In the southern Carajás Domain, (Canaã dos Carajás area) Xingu migmatites formed by partial melting of a TTG series gneiss protolith, after granulite facies metamorphism (Delinardo et al 2015). According to these authors, the Xingu migmatites register the collisional phase of an orogenic event developed ca 2.96 Ga (U-Pb upper intercept crystallization ages analyses of deformed leucosome).

In the northeastern Carajás Domain, this study area, the Xingu Migmatites (Britalider and Britamil metatexites and diatexites) and the Dark gray gneiss represent the product of regional metamorphism, as rocks typically formed in collisional orogens tectonic setting. In the northeastern Carajás Domain, granulite facies metamorphism and subsequent partial melting event took place within the ca. 2.88 to 2.85 Ga interval, wich is ca. 80 Ma younger than the southern Carajás Domain. Exceptionally for the Rio Verde Trondhjemite, which records a complex evolution between 2.93-2.85 Ga (Feio et al 2013), no other rocks formed during this time interval (2.96-2.88Ga) in the Carajás Domain were reported until now.

CONCLUSIONS

Detailed fieldwork and microstructural analysis allowed us to identify evidence of widespread anatexis in the northeastern area of the Carajás Domain. This study reveals a new migmatite occurrence (Britalider Quarry metatexites and diatexites) at the Carajás Province and provides new data that corroborate with the partial melting of the mesoarchean Xingu gneiss basement at two different localities (Britamil and Britalider quarries). The Xingu banded orthogneisses outcrops nearby the quarries area. These unmelted to incipiently melted rocks register metamorphic peak at upper amphibolite facies, which might correspond to the conditions developed near a hypothetical melt-in isograd.

The Xingu metatexites and diatexites morphologies and its constituent parts differ in each migmatite occurrence. The Britamil Quarry occurrence preserves most of the metamorphic structures, such as gneissic foliation. The leucosomes dominantly occur as in source veins and locally as nebulite diatexites. In the Britalider Quarry, stromatic metatexites preserve the banded structure of the protolith. The gain of melt promoted further disaggregation of amphibolite layers, producing schollen diatexites and developed schlieren diatexites at higher melting rates. Thus, apparently the former melt content increased towards north in the northeastern part of the Carajás Domain.

An integrate perspective considering migmatites morphologies, the amount of melt produced, rock microstructures and the protolith composition, indicates that partial melting was triggered by water influx synchronous to shearing. The petrological diversity of these two migmatites occurrences provide examples of how the water content and strain rates are as determinant as the protolith composition and temperature in melting of high-grade rocks.

The studied rock types typically form during collisional orogens, as products of regional metamorphism accompanied by the partial melting of the continental crust. In the Britamil Quarry, the Dark gray gneiss high-temperature mineral phases (Cordierite-Spinel) were stabilized during granulite facies metamorphism. In the Britalider Quarry advanced melting of tonalite layers developed voluminous diatexites bodies and led to the incipient amphibolite mesosome partial melting, forming more tonalitic melt with perithetic amphibole.

The Xingu gneisses and migmatites register a complex history, preserving trace elements geochemistry signatures from the igneous protolith MORB and TTG suites to their subsequent metamorphism during orogen accretionary phase (subduction zone influence). By its turn, petrography and geochronology data had better register the orogen collisional phase (high temperature metamorphism and partial melting) to post-collisional extension (melt crystallization and exhumation).

The individualization of Britamil and Britalider occurrences, combined with available data of the literature on migmatites supports substantial anatexis of the mesoarchean basement rocks in the Carajás Domain. The ages obtained in this study suggest zircon grains recrystallization at ca 2.88 to 2.86 Ga at high-grade metamorphic conditions. The evolution of the Carajás Domain during the Mesoarchean involves at least two major episodes of crustal recycling, at ca 2.96 Ga and 2.86 Ga. Until now, no rock formation has been reported between this time.

ACKNOWLEDGEMENTS

This research was funded by FAEPEX/PRP/UNICAMP (grant 519.292 – 0045/15), INCT/Geociam (CNPq/FAPESPA/Petrobras 573733/2008-2), FAPESP (grant 2016/13162-7), and CNPq (grant 457689/2014-5). We are grateful to the Geoscience Institute of the Federal University of Pará (UFPA), especially Prof. Dr. Davis Oliveira, for logistical support during fieldtrip and to Britamil and Britalider staff for facilities in accessing quarries. We also thanks laboratory technicians of Geoscience Institute of University of Campinas for support during data acquisition. Jackeline Monteiro Faustinoni thanks Capes for the master scholarship.

REFERENCES

Almeida, J.A.C., R. Dall´Agnol, M.A. Oliveira, M.J.B. Macambira, M.M. Pimentel, O.T. Rämö, F.V. Guimarães, and A.A.S. Leite. 2010. Zircon geochronology and geochemistry of the TTG suites of the Rio Maria granite-greenstone terrane: implications for the growth of the Archean crust of Carajás Province, Brazil. Precambrian Research (120):235-257.

Araújo, O.J.B., Maia, R.G.N. 1991. Serra dos Carajás, folha SB.22-ZA, Estado do Pará. Programa Levantamentos Geológicos Básicos do Brasil. Companhia de Pesquisa de Recursos Minerais

Ashworth, J.R. and McLellan, E.L. 1985. Textures. In Migmatites, Ashworth, J.R. (ed.) 180-203. Glasgow: Blackie.

Barker, F. 1979. Trondhjemite: a definition, environment and hypotheses of origin. In: Barker, F. (Ed.), Trondhjemites, Dacites and Related Rocks. Elsevier, Amsterdam, pp. 1–12.

Barker, F. and J.G. Arth. 1976. Generation of trondhjemite-tonalite liquids and Archean bimodal trondhjemite-basalt suites. Geology 4:596-600.

Barros C.E.M., Macambira M.J.B., Barbey P., Scheller T. 2004. Dados isotópicos Pb–Pb em zircão (evaporação) e Sm–Nd do Complexo Granítico Estrela, Província Mineral de Carajás, Brasil: implicações petrológicas e tectônicas. Rev. Brasil. Geoci. 34, 531–538

Barros, C.E.M., V.M. Nascimento, and C.A. Medeiros Filho. 2010. Revisão da estratigrafia das rochas de Serra Leste, Província Mineral de Carajás. Rev. Bras. Geoc. 40(2):167-174.

Berger, A., Burri, T., Alt-Epping, P., and Engi, M., 2007. Tectonically controlled fluid flow and water-assisted melting in the middle crust: An example from the Central Alps: Lithos, 18 p., doi: 10.1016/j.lithos.2007.07.027.

Binns, R. A.,- 1965. The mineralogy of metamorphosed basic rocks from the Willyama Complex, Broken Hill district, New South Wales. Min. Mag.,35: 306-326

Brown, M., 1994. The generation, segregation, ascent and emplacement of granite magma: the migmatite-to-crustally derived granite connection in thickened orogens. Earth- Science Reviews, 36, 83–130.

Brown, M., 2007. Crustal melting and melt extraction, ascent and emplacement in orogens: Mechanisms and consequences. Journal of the Geological Society 164, 709–730.

Brown, M. 2012. Open- and closed-system processes in the formation of migmatites and migmatitic granulites. J. Metam. Geol. Virtual special issue on crustal melting.

Brown, M. & Solar, G.S. 1997. Shear zone systems and melts: feedback relations and self-organization in orogenic belts. Journal of Structural Geology 20 (2-3), 211-217

Brown, M., Solar, G.S., 1998b. Granite ascent and emplacement during contractional deformation in convergent orogens. Journal of Structural Geology 20, 1365–1393.

Cann, J.R. 1970. Rb, Sr, Y, Zr and Nb in some ocean floor basaltic rocks. Earth and Planetary Science Letters 10: 7-11

Carvalho, B. B., Sawyer, E. W., Janasi, V. A., 2016. Crustal reworking in a shear zone: transformation of a metagranite to migmatite. J. Metam. Geol., 34 (3), 237-264. DOI: 10.1111/jmg.12180

Corfu, F., Hanchar, J.M., Hoskin, P.W.O., Kinny, P., 2003. Atlas of zircon textures: Reviews in Mineralogy and Geochemistry, v. 53, p. 469-500.

Delinardo da Silva, M. 2014. Metatexitos e diatexitos do Complexo Xingu na região de Canãa dos Carajás: implicações para a evolução mesoarquana do Domínio Carajás. P. 119 in Master Thesis. Campinas: UNICAMP.

Delinardo da Silva, M., L.V.S Monteiro, C.P.N Moreto, and S.S. Damasceno 2015. Metamorfismo e geoquímica do Complexo Xingu na região de Canãa dos Carajás: Implicações para a evolução Mesoarqueana do Domínio Carajás, Província Carajás. Pp. 279-298 in Contribuições à geologia da Amazônia.

Docegeo 1988. Revisão Litoestratigráfica da Província Mineral de Carajás-Litoestratigrafia e principais depósitos. Pp. 11-54 in 35º Congresso Brasileiro de Geologia. SBG.

Feio, G.R.L, R Dall'Agnol, , M.B. Macambira, A.C.B. Gomes, A.S. Sardinha, and P.A. Santos. 2012. Geochemistry, geochronology, and origin of the Neoarchean Planalto Granite suite, Carajás Amazonian craton: A-type or hydrated charnockitic granites. (http://dx.doi.org/10.1016/j.lithos.2012.02.020.).

Feio, G.R.L., R. Dall´Agnol, E.L. Dantas, M.J.B. Macambira, J.O.S. Santos, F.J. Altholff, and J.E.B. Soares. 2013. Archean granitoid magmatism in the Canãa dos Carajás area: implications for crustal evolution of the Carajás Province, Amazonian Craton, Brazil. Precambrian Research 227:157-185.

Frost, B.R., C.G. Barnes, W. Collins, R.J. Arculus, D.J. Ellis, and C.D., Frost. 2001. A geochemical classification for granitic rocks. Journal of Petrology 42:2033-2048.

Gao, X.Y., Zhang, Q.Q., Zheng, Y.F., Chen, Y.X., 2017. Petrological and zircon evidence for the Early cretaceous granulite-facies metamorphism in the Dabie orogeny - China. Lithos 284–285: 11–29

Hasalová, P., Stıpská, P., Powell, R., Schulmann, K., Janousek, V. & Lexa, O., 2008a. Transforming mylonitic metagranite by open-system interactions during melt flow. Journal of Metamorphic Geology, doi: 10.1111/j.1525-1314.2007.00744.x

Hasalová, P., Janousek, V., Schulmann, K., Stıpská, P. & Erban,V., 2008b. From orthogneiss to migmatite: geochemical assessment of the melt infiltration model in the Gfohl Unit (Moldanubian Zone, Bohemian Massif). Lithos, doi: 10.1016/j.lithos.2007.07.021

Hollister, L.S. and Crawford, M.L., 1986. Melt-enhanced deformation: A major tectonic process. Geology, v 14 p. 558-561

Holness, M.B., and Sawyer, E.W., 2008, On the pseudomorphing of melt-filled pores during the crystallization of migmatites: Journal of Petrology, v. 49, p. 13

Janousek, V., Farrow, C.M., Erban, V. 2006. Interpretation of whole-rock geochemical data in igneous geochemistry: introducing geochemical da Toolkit (GCDkit).Journal of Petrology, 47: 1255-1259.

Kriegsman, L.M., and Hensen, B.J. 1998. Back reaction between restite and melt: Implications for geothermobarometry and pressure– temperature paths. Geology, 26: 1111–1114.

Kunz, B.E., Johnson, T.E., White, R.W., Redler, C., 2014. Partial melting of metabasic rocks in Val Strona di Omegna, Ivrea Zone, northern Italy Lithos 190:1-12

Lee, Y. & Cho, M., 2013. Fluid-present disequilibrium melting in Neoarchean arc-related migmatites of Daeijak Island, western Gyeonggi Massif, Korea. Lithos 179:249-262 doi: 10.1016/j.lithos.2013.08.011

Machado, N., D.H. Lindenmayer, T.E. Krough, and Z.G. Lindemayer. 1991. U-Pb Geochronology of Archean magmatism and basement reactivation in the Carajás Area, Amazon Shield, Brazil. Precambrian Research 49:329-354.

Martin, H. 1994. The Archean gray gneisses and the gneisses of continental crust. Pp. 205-259 in Developments in Precambrian Geology.Archean Crustal Evolution, edited by K.C. Condie. Amsterdam: Elsevier.

Mcdounogh, W.F. and S.S. Sun. 1995. The composition of the Earth. Chemical Geology 120:223-253.

Melo, G.H.C., Monteiro, L.V.S., Xavier, R.P., Moreto, C.P.N., Santiago, E.S.B., Dufrane, A.S., Aires, B. Santos, F.F.A., 2016. Temporal evolution of the giant Salobo IOCG deposit, Carajás Province (Brazil): constraints from paragenesis of hydrothermal alteration and U-Pb geochronology. Miner Deposita Springer doi: 10.1007/s00126-016-0693-5

Mogk, D.W., 1992. Ductile shearing and migmatization atmidcrustal levels in an Archean high-grade gneiss belt, Northern Gallatin Range, Montana, USA. Journal of Metamorphic Geology 10, 427–438.

Monteiro, L.V.S.;Xavier, R. P.;Souza Filho, C. R.;Moreto, C. P. N., 2014. Metalogenia da Província Carajás. In: Silva M.G.; Jost H.; Kuyumajian R.M.. (Org.). Metalogênese das Províncias Tectônicas Brasileiras. 1ed.: CPRM, V. 1, p. 1-50.

Moreto, C.P.N., L.V.S Monteiro, R.P. Xavier, W.S. Amaral, T.J.S. dos Santos, C. Juliani, and C.R. Souza-Filho. 2011. Mesoarchean (3.0 and 2.86 Ga) host rocks of the iron oxide-Cu-Au Bacaba deposit, Carajás Mineral Province: U-Pb geochronology and metallogenetic implications. *Mineralium Deposita* 46:789-811.

Moreto, C.P.N., L.V.S. Monteiro, R.P. Xavier, R.A. Creaser, S.A. Dufrane, G.H.C. Melo, M.A. Delinardo da Silva, C.C.G. Tassinari, and K. Sato. 2015a. Timing of multiple hydrothermal events in the iron oxide–copper–gold deposits of the Southern Copper Belt, Carajás Province, Brazil. *Mineral Deposita* (50):517-546.

Moreto, C.P.N., L.V.S. Monteiro, R.P. Xavier, R. Creaser, A. Dufrane, C.G. Tassinari, K. Sato, A.I.S. Kemp, and W.S. Amaral. 2015b. Paleoproterozoic overprint on Archean iron oxide-copper-gold system at the Sossego deposit, Carajás Province: Re-Os and U-Pb geochronological evidence. *Econ. Geol.* 110:809-835.

Moyen, J-F. 2011. The composite Archean grey gneisses: petrological significance, and evidence for a non-unique tectonic setting or Archean crustal growth. Lithos, 123:556-574.

Nakamura, N. 1974. Determination of REE, Ba, Fe, Mg, Na, and K in carbonaceous and ordinary chondrites. Geochem. Chosmochem. Acta 38(757-775).

Navarro, M.S., Andrade, S., Ulbrich, H., Gomes, C.B., Girardi, V.A.V., 2008. The direct determination of rare earth elements in basaltic and related rocks using ICP-MS: testing the efficiency of microwave oven sample decomposition procedures. Geostand Geoanal Res.;32:167–80

O´Connor, J.T. 1965. A classification for quartz-rich igneous rocks based on feldspar ratios. US Geological Survey Professional Papers 525:79-84.

Palin, R.M., White, R.W., Green, E.C.R., Diener, J.F.A., Powell, R., Holland, T.J.B., 2016b. High-grade metamorphism and partial melting of basic and intermediate rocks. Journal of Metamorphic Geology, v. 34, p. 871–892, doi: 10.1111/jmg.12212.

Pattison, D.R.M., Chacko, T., Farquhar, J. & McFarlane, C.R.M., 2003. Temperatures of granulite-facies metamorphism: constraints from experimental phase equilibria and thermobarometry corrected for retrograde exchange. Journal of Petrology 44, 867-900.

Pearce, J.A., N.W. Harris, and A.G. Tindle. 1984. Trace element discrimination diagrams for the tectonic interpretation of granitic rocks. *Journal of Petrology* 25:956-983.

Pearce, J.A., 2014. Immobile element fingerprinting of ophiolites. *Elements* 10:101-108.

Pidgeon, R. T. (1992) Recrystallisation of oscillatory zoned zircon: some geochronological and petrological implications. Contributions to Mineralogy and Petrology, v. 110, n. 4, p. 463-472.

Pidgeon, R.T., M.J.B. Macambira, and J.M. Lafon. 2000. Th–U–Pb isotopic systems and internal structures of complex zircons from an enderbite from Pium Complex, Carajás Province, Brazil: evidence for the ages of granulite facies metamorphism and the protolith of the enderbite. *Chem. Geol.* (166):159-171.

Pinheiro, R.V.L. and R.E. Holdsworth. 2000. Evolução tectono-estratigráfica dos sistemas transcorrentes Carajás e Cinzento, Cinturão Itacaiúnas, na borda leste do Cráton Amazônico. *Revista Brasileira de Geociências* (30):597-606.

Prince, C., Harris, N., Vance, D., 2001. Fluid-enhanced melting during prograde metamorphism. Journal of the Geological Society 158, 233–242.

Ricci, P.S.F. and M.A. Carvalho 2006. Rocks of the Pium-Area, Carajás Block, Brazil – A deep seated high-T gabbroic pluton (charnockitoid-like) with xenoliths of enderbitic gneisses dated at 3002 Ma – the basement problem revisited. in *8ºSimpósio de Geologia da Amazônia*. Manaus.

Rubatto, D .,2002. Zircon trace element geochemistry: partitioning with garnet and the link between U–Pb ages and metamorphism. Chemical Geology 184: 123-138

Rubato, D. 2017 Zircon: The metamorphic mineral. Reviews in Mineralogy and geochemistry. V.83 doi:10.2138/rmg.2017.83.09

Rubatto, D. & Hermann, J., 2007b. Zircon behaviour in deeply subducted rocks. Elements 3:31–35

Rudnick, R. L. 1992. Restites, Eu anomalies and the lower continental crust. Geochimica et Cosmochimica Acta, 56:963- 970, doi: 10.1016/0016-7037(92)90040-P.

Santos, J.O.S., L.A. Hartmann, H.E. Gaudette, D.I. Groves, N.J. Mcnaughton, and I.R. Fletcher. 2000. A new understanding of the Provinces of the Amazon Craton based on integration of field mapping and U-Pb and Sm-Nd geochronology. *Gondwana Research* 453-488.

Santos, J.O.S. 2003. Geotectônica do Escudo das Guianas e Brasil-Central. Pp. 169-226 in Geologia, tectônica e recursos minerais do Brasil: texto, mapas e SIG. Brasília.

Santos, R. D., Galarza, M. A., Oliveira, D. C. 2013c. Geologia, geoquímica e geocronologia do Diopsídio-Norito Pium, Província Carajás. Boletim do Museu Paraense Emílio Goeldi, Ciências Naturais, 8(3), 355-382.

Sardinha, A.S., C.E.M. Barros, and M. Krymsky. 2006. Geology, geochemistry and U–Pb geochronology of the Archean (2.74 Ga) Serra do Rabo granite stocks, Carajás Metallogenetic Province, northern Brazil. J. S. Am. Earth Sci. (20):327-339.

Sawyer, E.W. 1991. Disequilibrium melting ond the rate of melt-residuum separation during migmatization of mafic rocks from the Grenville Front, Quebec. Journal of Petrology, 32: 701-738.

Sawyer, E. W. (1994), Melt segregation in the continental crust, Geology, 22, 1019–1022

Sawyer, E.W., 1999. Criteria for the recognitionof partial melting. Physics and Chemistry of Earth, 24: 269-279.

Sawyer, E.W., 2001. Melt segregation in the continental crust: distribution and movement of melt in anatetic rocks. Journal of Metamorphic Geology, 19: 291-309.

Sawyer, E.W. 2010., Migmatites formed by water-fluxed partial melting of a leucogranodiorite protolith: microstructures in the residual rocks and source of the fluid.Lithos, 116: 273-286.

Sawyer, E. W. and Brown, M., 2008. Working with Migmatites. Quebec: Mineralogical Association of Canada.

Shand, S.J. 1943. Eruptive rocks. Their Genesis, Composition, Classification, and their Relation to Ore Deposits, with a chapter on Meteorites. 2nd ed. New York: Hafner Publishing Co.

Siebel, W., Eroglu, S., Shang, C., Rohrmuller, J., 2012. Zircon geochronology, elemental Sr-Nd isotope geochemistry of two variscan granitoids. Miner. Petrol. doi: 10.1007/s00710-012-0200-3

Silva, G.G., M.I.C. Lima, A.R.F. Andrade, R.S. Issler, and G. Guimarães 1974. Geologia. in DNPM. Projeto Radam. Folha SB.22 Araguaia e parte da folha SC22 Tocantins: geologia, geomorfologia, solos, vegetação e uso potencial da terra. Rio de Janeiro.

Song, Y., Xu, H., Zhang, J., Wang, D., Liu, E., 2014. Syn-exhumation partial melting and melt segregation in the Sulu UHP terrane: Evidences from leucosome and pegmatitic vein of migmatite. Lithos, 202-203, p. 55-75. doi:10.1016/j.lithos.2014.05.017

Spear, F.S., 1993. Metamorphic Phase Equilibria and Pressure-Temperature-Time Paths. Mineralogical Society of America, Washington, D.C., 799pp.

Sun, S.S and W.F. McDonough. 1989. Chemical and isotopic systematics of oceanic basalt; implications for mantle compositions and processes. Geological Society of London Special publication 42:313-345.

Tassinari, C.C.G and M.J.B. Macambira. 1999. Geochronological Provinces of the Amazonian Craton. Episodes 22:174-182.

Tassinari, C.C.G. and M.J.B. Macambira 2004. A evolução tectônica do Cráton Amazônico. Pp. 471-485 in Geologia do Continente Sul-americano: evolução da obra de Fernando Flávio Marques de Almeida, edited by V. Mantesso-Neto, A. Bartorelli, C.D.R. Carneiro, and B.B. Brito Neves. São Paulo: Beca.

Tavares, F.M. 2015. Evolução Geotectônica do Nordeste da Província Carajás. University of Rio de Janeiro, PhD thesis.

Timmermann, H., Jamieson, R. A., Parrish, R. R., Culshaw, N. G., 2002. Coeval migmatites and granulites, Muskoka domain, southwestern Grenville Province, Ontario. Canadian Journal of Earth Sciences. 39, 239–258.

Timms, N.E., Kinny, P.D., Reddy, S.M., 2006. Deformation-related modification of U and Th in zircon. Geochim Cosmochim Acta 70:A651

Vasquez, M.L., L.T. Rosa-Costa, C.G. Silva, P.F. Ricci, J.O. Barbosa, E.L. Klein, E.S. Lopes, E.B. Macambira, C.L. Chaves, J.M. Carvalho, J.G Oliveira, G.C. Anjos, and H.R. Silva. 2008. Geologia e recursos minerais do Estado do Pará, Sistema de Informações Geográficas. Belém.

Vendemiatto, M.A., Enzweiler, J., 2001. Routine control of accuracy in silicate rock analysis by X-ray fluorescence spectrometry. Geostandards Newsletter The Journal of Geostandards and Geoanalysis 25:283-291.

Vernon, R.H. 2008. A pratical guide to rock microstructure. 2nd ed. Cambridge.

Vernon, R.H.,2011. Microstructures of melt-bearing regional metamorphic rocks. In van Reenen, D.D., Kramers, J.D., McCourt, S., and Perchuk, L.L., eds., Geological Society of America. doi: 10.1130/2011.1207(01)

Vielzeuf, D., Clemens, J.D., Pin, C., E Moinet, E., 1990. Granites, granulites and crustal differentiation. In: Granulites and crustal evolution. Springer Netherlands, 59-85 p.

Waters, D.J., 1991. Hercynite-quartz granulites: phase relations, and implications for crustal processes European Journal of Mineralogy, V. 3 (2) p. 367 - 386 doi:10.1127/ejm/3/2/0367

Watkins, J.M., Clemens, J.D.,Treloar, P.J., 2007. Archaean TTGs as sources of younger granitic magmas: melting of sodic metatonalites at 0.6–1.2 GPa. Contributions to Mineralogy and Petrology, 154, 91–110.

Weinberg, R. F., Veveakis, M. & Regenauer-Lieb, K., 2015. Compaction-driven melt segregation in migmatites. Geology. 43, 6, p. 471-474

Weinberg, R.F., 2016. Himalayan leucogranites and migmatites: nature, timing and duration of anatexis. J. metamor. geol. v34, 8,p. 821-843.

Weinberg, R.F. & Hasalova, P., 2015. Water-fluxed melting of the continental crust: a review. Lithos, 212–215, 158–188.

White, R.W., Pomroy, N.E., Powell, R., 2005. An in situ metatexite–diatexite transition in upper amphibolite facies rocks from Broken Hill, Australia. J. Metamor. Geol, 23, 579-602. doi:10.1111/j.1525-1314.2005.00597.x

White, R.W., Palin, R.M., Green, E.C.R., 2017. High-grade metamorphism and partial melting in Archean composite grey gneiss complexes. J. Metam. Geol, 35, 181-195. doi:10.1111/jmg.12227

White, R.W., Powell, R. 2010. Retrograde melt–residue interaction and the formation of near-anhydrous leucosomes in migmatites. Journal of Metamorphic Geology, 28:579–597.

Zhang, Z., Dong, X., Xiang, H., Ding, H., He, Z., Liou, J., 2014. Reworking of the Gangdese magmatic arc, southeastern Tibet: Post-collisional metamorphism and anatexis. J. of Metamor. Geol., 33(1), doi: 10.1111/jmg.12107